

ROYAL SOCIETY
OPEN SCIENCE

rsos.royalsocietypublishing.org

Research



Article submitted to journal

Subject Areas:

Robotics, Artificial Intelligence,
Biomimetics

Keywords:

Swarm Robotics, Multi-Robot
Systems, Fault Tolerance,
Bio-Inspiration

Author for correspondence:

James O'Keefe

e-mail:

james.okeefe@york.ac.uk

THE ROYAL SOCIETY
PUBLISHING

Detecting and Diagnosing Faults in Autonomous Robot Swarms with an Artificial Antibody Population Model

James O'Keefe

Department of Computer Science, University of
York, United Kingdom

An active approach to fault tolerance is essential for long term autonomy in robots – particularly multi-robot systems and swarms. Previous efforts have primarily focussed on spontaneously occurring electro-mechanical failures in the sensors and actuators of a minority sub-population of robots. While the systems that enable this function are valuable, they have not yet considered that many failures arise from gradual wear and tear with continued operation, and that this may be more challenging to detect than sudden step changes in performance. This paper presents the Artificial Antibody Population Dynamics (AAPD) model – an immune-inspired model for the detection and diagnosis of gradual degradation in robot swarms. The AAPD model is demonstrated to reliably detect and diagnose gradual degradation, as well as spontaneous changes in performance, among swarms of robots of as few as 5 robots while remaining tolerant of normally behaving robots. The AAPD model is distributed, offers supervised and unsupervised configurations, and demonstrates promising scalable properties. Deploying the AAPD model on a swarm of foraging robots undergoing slow degradation enables the swarm to operate at an average of 79% of its performance in perfect conditions.

1. Introduction

A significant barrier to the real-world deployment of autonomous robots, particularly in environments that are populated, uncontrolled, difficult to access, and/or safety-critical, is the risk of failure or loss of autonomous control in the field. These risks compound for multi-robot systems (MRS), where there is additional vulnerability to faults and failures in the interaction space between agents.

© 2014 The Authors. Published by the Royal Society under the terms of the Creative Commons Attribution License <http://creativecommons.org/licenses/by/4.0/>, which permits unrestricted use, provided the original author and source are credited.

Swarm robotic systems (SRS), a variant of MRS, are suited to spatially distributed tasks – particularly in dangerous/inaccessible environments – because of their redundancy of hardware and distributed control architectures, meaning that there is no single point of failure [1]. In their seminal paper on swarm robotics, Şahin [1] proposes that these properties provide robot swarms with an innate robustness – that is, the ability to tolerate faults and failures in individual robots without significant detriment to the swarm as a whole. However, later studies [2] demonstrate that failures in individual robots can significantly disrupt overall swarm performance – particularly where a partially failed robot is able to maintain a communication link with other robots and influence their behaviour. Further investigation [3] concludes that an active approach to fault tolerance is necessary if robot swarms are to retain long-term autonomy, and specifically highlights artificial immune systems (AIS) as a promising solution.

One of the defining characteristics of the natural immune system, and one of the most desirable properties for transferring to engineered systems, is its ability to learn and remember infections it has previously encountered and to detect and destroy those infectious cells more efficiently on subsequent encounters. *Maintenance* is defined by Cohen [4] to be the property of the natural immune system that enables it to protect its host against harm it will receive during its life, and comprises three stages: Recognition, cognition, and action. Previous research has mapped these to three stages of active fault tolerance in engineered systems: Fault detection, fault diagnosis, and recovery (FDDR) [5] [6].

Previous work towards fault tolerance in MRS/SRS has mostly examined individual elements of FDDR in isolation by spontaneously injecting sensor and actuator faults into a sub-population of individual robots and then attempting to detect, diagnose, and/or resolve the failed robot(s) reactively (i.e. once the afflicted robot has already failed to a problematic degree). While modelling faults as spontaneous events is appropriate for some kinds of fault, e.g. a robot that is immobilised suddenly after becoming stuck on an obstacle, other types of fault occur gradually. An example of this would be the accumulation of dust and debris on motor and sensor hardware, highlighted in the real-world study by Carlson et. al. [7]. This type of fault modelling has been hitherto missing in SRS/MRS fault tolerance literature and presents an opportunity to implement autonomous fault tolerance as a predictive measure, rather than a reactive one. By detecting early-stage degradation on robot hardware before reaching a critical failure point, an at-risk robot can be allowed a grace period in which to return itself to a controlled area for receiving maintenance. Such an approach could lead to the reduction and/or prevention of failure or loss of autonomous control in the field – a significant advantage for many real-world scenarios.

This paper presents the Artificial Antibody Population Dynamics Model (AAPD-Model), a system for the detection and diagnosis of potential faults and hazards which aims to approximate the self-tolerance and learning properties of the adaptive immune system. The AAPD-Model is based on Farmer et al.'s [8] model of antibody population dynamics and is tested on a simulated SRS in this work.

The contributions of this paper are as follows:

- A novel distributed bio-inspired algorithm for the autonomous detection and diagnosis of potential faults in SRS that can accommodate supervised and unsupervised configurations.
- The first instance of integrated fault detection and diagnosis in SRS
- Novel modelling of SRS hardware faults as gradual degradation

The rest of this paper is structured as follows: Section 2 gives a review of relevant literature in the field of fault tolerant MRS/SRS and summarises with some of the open questions this paper seeks to address. Section 3 describes the experimental testbed used for this work and some preliminary experiments for system design and parameterisation. Section 4 describes the design and implementation of the AAPD Model in SRS. Section 5 details the experiments performed to test the performance of the AAPD Model, including results and discussion. Section 6 concludes this paper and lists avenues for future work.

2. Related Work

There is a vast body of literature on FDDR in engineered systems. For brevity, this section highlights the comparatively smaller body of relevant work on SRS and MRS detection and diagnosis of electro-mechanical faults.

Fault Detection

Fault detection typically compares observed behaviour with a predefined model of expected behaviour (model-based approaches), or against system models that are built in real-time from observations during operation (data-driven approaches), where discrepancies and outliers indicate potential faults [9].

Khadidos et al. [10] devise a system whereby each robot in a swarm broadcasts information from its sensors, position coordinates and motor values to its neighbours and estimates their positions relative to itself. Discrepancies between estimated and reported locations are reported as suspicious, at which point a third robot acts as an independent adjudicator.

Millard [5] detects electro-mechanical faults in individual robots by comparing the robot's observed behaviour with the outputs of simulated copies of its controller.

Strobel et al. [11] demonstrate a blockchain-based system for detecting byzantine robots in a swarm (where byzantine can mean malfunctioning or malicious). Strobel et al. implement a token economy whereby robots are allocated tokens that allow them to participate in the swarm's critical activities according to their contributions. Byzantine robots quickly run out of tokens when their performance drops, preventing them from influencing the rest of the swarm.

Tarapore et al. [12] use an immune-inspired outlier detection model (based on the crossregulation model (CRM) [13]) for detecting faults in robot swarms. Tarapore et al. encode individual robot behavioural states as binary feature vectors (BFVs), where each feature indicates whether a particular state is true or false (e.g. whether angular velocity is greater than a threshold value). These BFVs are then fed into the CRM model.

Fault Diagnosis

Different types of fault cause robots to fail in different ways, degrading performance at the individual robot and swarm levels with varying degrees of severity. Diagnosing a fault determines the appropriate resolution and the urgency with which it should be carried out.

In MRS, Daigle et al. [14] use discrepancies between observed and model-predicted robot behaviour to create signatures for different electro-mechanical fault types that can be used to diagnose in real-time. Similarly, Carrasco et al. [15] build models of normal and faulty behaviour offline which are then used for online detection and diagnosis of faults based on which model most closely corresponds to measured robot states. Kutzer et al. [16] use diagnostic manoeuvres, consisting of various tests designed to isolate the root-cause of a fault, and a trained probabilistic model to estimate the state of the faulty robot based on its performance of the manoeuvres.

In SRS, the author's previous work in software [6] and hardware [17] demonstrates an immune-inspired diagnosis system. Electro-mechanical faults are initially diagnosed using an exhaustive series of diagnostic manoeuvres that associate a fault type with a behavioural signature and commit it to memory. When subsequent faults are detected, they can be diagnosed according to the statistical similarity between their behavioural signatures and the repertoire of recent behavioural signatures stored in memory.

Summary

The literature discussed in this section describes a variety of approaches to the detection and diagnosis of electro-mechanical faults in MRS/SRS. Each approach considers detection or diagnosis in isolation, and considers faults which occur suddenly and spontaneously.

Of the approaches to fault detection in SRS discussed, each system has been exogenous and data-driven – robots detect faults in others by exploiting the multiplicity of the swarm to create an implicit and variable

model of normal behaviour and from there detect outlying behaviours. Such approaches benefit from real-time flexibility, but are limited insofar that a majority population must always be operating normally. This would prevent the detection of faults or failures induced by external factors (i.e. difficult terrain or hazardous environmental conditions) affecting a majority of robots, despite such failures being equally deserving of detection and mitigation strategies. Furthermore, each approach considers the normally behaving majority to be operating at full capacity, while a minority sub-population suffers faults that are distinctly recognisable among the normally operating population – e.g. implementations in which a partially failed motor operates at 50% output or a completely failed motor that produces no output [12] [6]. This does not consider that each robot has its own independent MTBF and that, rather than binary faulty/non-faulty states, within the swarm there may be represented a wide range of partially functioning robots (e.g. covering the 0 - 100% output spectrum). It has been so far unclear whether data-driven outlier detection approaches to fault tolerance would succeed in such cases.

The discussed approaches to fault detection in SRS are not able to learn, remember, or improve over time. Unsupervised learning is demonstrated in previous work on SRS fault diagnosis [6], but relies on an assumption that individual robots can autonomously make fine behavioural assessments on other robots and carry out *in situ* repairs that are beyond the sensing and actuating abilities of most untethered mobile robots at the time of writing (particularly SRS platforms).

A key assessment criteria for the AAPD model will therefore be its ability to distinguish faulty or degraded robots from among a swarm operating in a range of tolerable but imperfect states, and whether or not this can be used as the basis for a process of unsupervised learning such that the reliability and efficiency of detection improves over time.

3. Experimental Test Bed

All of the research and experiments detailed in the following sections were conducted in software simulation using Robot Operating System (ROS) 2, Gazebo Classic, and MATLAB 2022.

To assist the reader, Table 1 lists all of the symbols used in this paper, along with their definitions.

Case Study

This work considers a swarm of simulated TurtleBot3 robots [18] that perform autonomous foraging (Algorithm 1), a common benchmark algorithm in swarm research [19], in an enclosed arena measuring 10m by 10m. Each robot must retrieve a resource from one of three circular resource nests with a radius of 1m, distributed evenly at arena (x,y) coordinates (2,8), (5,8), and (8,8), respectively. The resource must then be returned to an area denoted as the ‘base’, which spans the entire x dimension of the arena up to $y = 2$. In each experiment, robots are distributed evenly along the line $y = 2$ and about the midpoint (5,2). This can be seen in Figure 1. The base is the only region of the environment in which a robot is assumed to be able to interact with any external system (e.g. a robot arm, a human operator, etc.). Robots must return to base in order to receive charge or maintenance work. If a robot depletes its power or degrades to a point of immobility outside of the base, it is considered lost and becomes an obstacle for the remainder of an experiment.

The TurtleBot3 is a two-wheeled differential drive robot with open source models for simulated experimentation in ROS and Gazebo. Simulated robots are provided with the ability to detect other robots and objects up to 4 metres away. The basis for this decision is ultrasonic sensors which have been previously used for decentralised and accurate swarm localisation, the details of which can be found in [20]. Ultrasonic sensors are a good experimental base for SRS research since they are cheap, energy efficient, enforce a limited local sensing area, and are susceptible to gradual build up of dust and debris causing sensor inertia and reducing sensing range over time. The standard deviation of Gaussian noise applied to each sensor measurement is set to be 5% of the true value. This is a relatively harsh implementation of error that is selected to test the robustness of the system and the AAPD model – modern ultrasonic sensors can typically achieve sub-cm accuracy within 3m [21].

Symbol	Meaning	Value or reference
N	Gaussian noise about mean μ with standard deviation σ	$\mu = 0$ in all cases.
N	The number of robots in a SRS	$1 \leq N \leq 10$
R_{1-N}	A robot within a SRS of size N	
I_{signal}	Intensity of transmitted signal	Equation 3.1
I_{min}	Minimum detectable signal intensity	Equation 3.2
P_{signal}	Power of transmitted signal	Equation 3.1, Equation 3.2
r	Range of transmitted signal	Equation 3.2
r_{max}	Maximum detectable range of transmitted signal	$4m$
P_{max}	Maximum robot power capacity	1 or ∞
v_{max}	Maximum linear velocity of robot wheel.	$0.22ms^{-1}$
$v_{l,r}$	Linear velocity of left and right robot wheels, respectively.	Equation 3.5
v	Linear velocity of robot.	$\frac{1}{2}(v_l + v_r)$
a	Axial separation of left and right robot wheels.	$16cm$
ω	Angular velocity of robot.	$\frac{1}{2}(v_l - v_r)$
r_{max}	Maximum transmission range of range and bearing sensor.	$4m$
AP_{max}	Maximum rate of power consumption by robot	$\frac{300}{s}$
AP	Rate of power consumption by robot	$AP_s + AP_l + AP_r$
$AP_{l,max,r,max}$	Rate of power consumption by left and right motors at maximum load, respectively.	$\frac{2}{3}AP_{max}$
$AP_{l,r}$	Rate of power consumption by left and right motors, respectively.	Equation 3.4
AP_S	Rate of power consumption by sensing and communication	$\frac{1}{2}AP_{max} + N$
$d_{l,r}$	Degradation severity coefficient on left and right wheels, respectively.	[0,1]
d_S	Degradation severity coefficient on localising signal transmitter.	[0,1]
d_0	The ideal value of $d_{l,r,s}$ at which to detect a robot as faulty	≈ 0.75 (Figure 3)
X	The repertoire of all artificial antibody populations for a single robot	
X_M	The repertoire of artificial antibody populations for motor hardware	
X_S	The repertoire of artificial antibody populations for sensor hardware	
Y	An artificial antigen repertoire shared by the SRS	
Y_M	An artificial antigen repertoire (motor hardware)	
Y_S	An artificial antigen repertoire (sensor hardware)	
x_i	The antibody population of type i	Equation 4.1, Equation 4.4, Equation 4.5
x_M	An artificial antibody population for motor hardware (within X_M)	
x_S	An artificial antibody population for sensor hardware (within X_S)	
y_j	The antigen population of type j	
y_M	An artificial antigen for motor hardware (within Y_M)	Equation 4.1, Equation 4.5
y_S	An artificial antigen for sensor hardware (within Y_S)	
p_j	The paratope of an artificial antibody or antigen of type j	
f	The fault threshold above which any artificial antibody population is detected as faulty by the AAPD model	1
δ	The value of $d_{l,r,s}$, whichever is smallest, at which an artificial antibody population is simulated above threshold f	
m	The matching specificity between two paratopes	Equation 4.2, Equation 4.3
s	A threshold to enforce a minimum matching specificity between two paratopes (not to be confused with s^{-1} , denoting per second, used elsewhere in this table).	Equation 4.2, Equation 4.3
W	The recording of robot sensor and state data over a recent temporal window.	
Ψ_T	The time in which a robot is correctly detected as faulty as a proportion of the total experimental time it spends in a faulty state	
Ψ_F	The time in which a robot is incorrectly detected as faulty as a proportion of the total experimental time it spends in a non-faulty state	

Table 1. Commonly used symbols used in this paper.

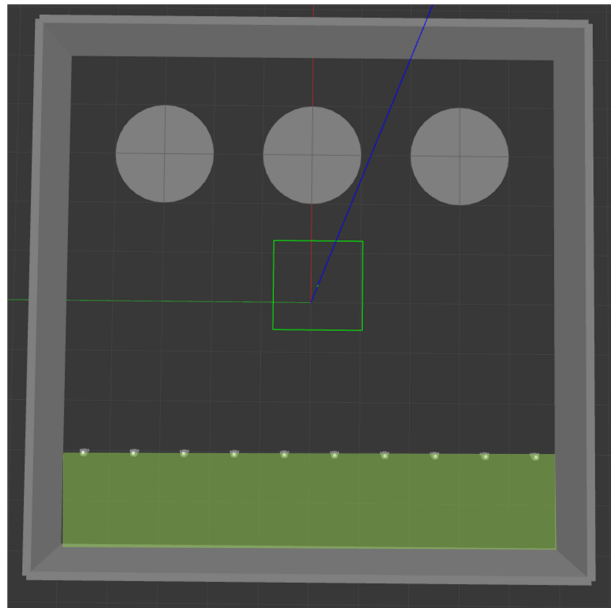


Figure 1. Experimental setup for 10 robots performing Algorithm 1 in an enclosed environment. Resource nests are indicated by the three grey circles opposite the robots. The highlighted green area indicates the robot base.

Electro-Mechanical Modelling

The sensing, communication, and locomotion functions performed by each robot consume power and are affected by degradation at different rates. A proportional model of power consumption is utilised whereby

Algorithm 1 Foraging Algorithm

```

1: while Running do
2:   if Object Distance  $\leq 0.5m$  then avoid
3:   else if Resource collected or Battery low or Faulty then Return to base
4:   if Robot at base then Deposit resource
5:   if Battery low then Recharge
6:   if Faulty then Repair
7:   else if Distance to centre of nearest Resource Nest  $\leq 0.75m$  then Collect resource
8:   else if Distance to nearest Resource Nest  $\leq r$  then Approach nearest resource
9:   else Move forwards

```

each robot is initialised with maximum power $P_{max} = 1$ and each process consumes a percentage of the robot's maximum power output, ΔP_{max} , per unit time. It is expected that locomotion consumes significantly more power than sensing, communication, and other background processes. Power consumption for a robot with both motors drawing maximum load, the most power consuming state it can take, is therefore modelled as a 20:40:40 split between power consumed by sensing, communication, and other background processes, power consumed by the left motor, and power consumed by the right motor, respectively. $\Delta P_{max} = \frac{1}{300}$ so that a robot drawing maximum power can operate for a total 5 minutes of simulated time.

Degradation caused by gradual wear, the accumulation of dust and debris, and adverse environmental conditions is simulated via a degradation severity coefficient $d_{l,r}$ on left and right motors, respectively, and d_S on simulated ultrasonic transmitter. Degradation affects physical processes and the power consumed by them. $d_{l,r}$ and d_S (Table 1), can take any value between 0 and 1, with 1 indicating perfect condition and 0 indicating that the corresponding hardware is completely degraded. The power consumption and degradation models for sensing, communication, and locomotion are as follows.

Sensing and Communication

Each robot is constantly emitting data and receiving data from other robots. Since transceiver outputs are not governed by corrective feedback loops in this case, the power consumed by robot sensing hardware and background processes, ΔP_S , is not expected to vary outside of a normal range. ΔP_S is therefore modeled as a constant with added Gaussian noise Table 1.

Degradation on the robot sensor, or environmental variations that result in higher levels of signal attenuation, will affect the maximum sensing range. This is modelled according to the inverse square law:

$$I_{signal} \propto \frac{P_{signal}}{r^2} \quad (3.1)$$

The maximum range of the sensor transmitter, r_{max} is taken to correspond to the minimum signal intensity, I_{min} , that can be reliably detected and localised by another robot. Signal intensity is proportional to transmitter inertia, and so the reduction in maximum detectable signal range caused by d_S is modelled as Equation 3.2.

$$r_{max} \propto \sqrt{\frac{(d_S)P_{signal}}{I_{min}}}, \text{ where } r = r_{max} \text{ for } d_S = 1 \quad (3.2)$$

Substituting, Equation 3.2 can be expressed as Equation 3.3:

$$r = r_{max} \sqrt{d_S} \quad (3.3)$$

Equation 3.3 is plotted in Figure 2A.

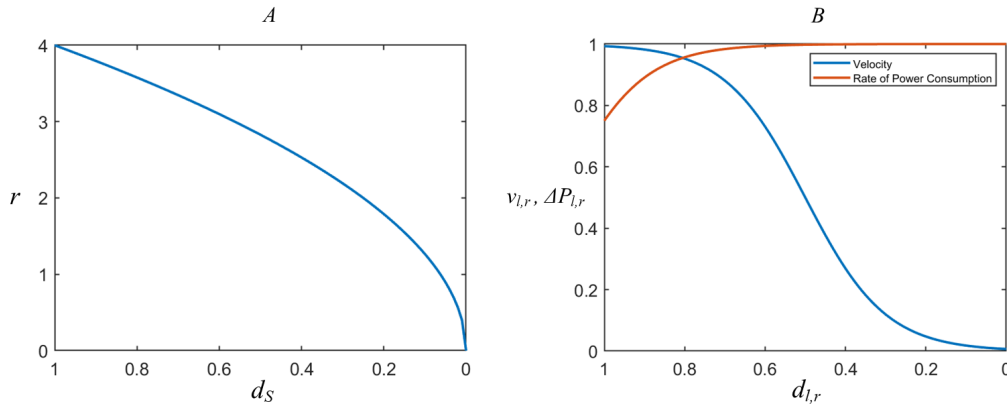


Figure 2. A: Robot sensing range r plotted against degradation severity coefficient d_S . **B:** Velocity and power consumption of left or right wheels, $v_{l,r}$ and $\Delta P_{l,r}$, respectively, normalised and plotted against degradation severity coefficients $d_{l,r}$.

Differential Drive

The power consumed by robot locomotion will be affected by the condition of its wheels and motors. Motors are typically designed to run at 50% - 100% of rated load, with maximum efficiency at around 75% [22]. A robot in perfect conditions is therefore taken to cause its motors to operate at 75% load.

The mechanical power required to achieve a given robot velocity is proportional to the forces incident upon it. As dust and debris accumulate on motor hardware, the friction generated will increase the mechanical power required to maintain a given velocity. A study into the reliability of motors over time plots the relationship as an approximately sigmoidal function [23]. Since the reliability and efficiency of a motor are directly related [22], the effects of motor degradation on robot locomotion are modelled thus:

The rate of power consumption, $\Delta P_{l,r}$, by left and right motors, respectively, is given by Equation 3.4.

$$\Delta P_{l,r} = \frac{\Delta P_{l_{max},r_{max}}}{1 + e^{-10((1-d_{l,r})+0.11)}} \quad (3.4)$$

where values of constants are set such that $P_{l,r} \approx 0.75\Delta P_{l_{max},r_{max}}$ for $d_{l,r} = 0$.

As the value $d_{l,r}$ increases, the mechanical power required to maintain robot velocity will eventually become greater than can be supplied. At this point, degradation will begin to reduce a robots maximum achievable velocity. Robot velocity is modelled as:

$$v_{l,r} = \frac{v_{max}}{1 + e^{-5(2d_{l,r}-1)}} \quad (3.5)$$

where values of constants are set to give the intersection of $v_{l,r}$ and $\Delta P_{l,r}$ as plotted in Figure 2B.

Scheduling Maintenance

Fault tolerance measures should seek to minimise robot downtime by detecting and resolving faults only as needed. In order to produce a system that performs this function autonomously, the point of degradation, or the values of $d_{l,r,S}$, at which continuing operation yields diminishing returns from individual robot performance must be identified. To this end, an initial set of experiments are conducted with a simulated swarm of 10 robots performing Algorithm 1 for 15 minutes of simulated time. Each robot is initialised with a random and independent probability between 0 - 15% of each degradation severity coefficient, d_l , d_r , and d_S , decrementing by 0.01 per second of simulated time. The total number of resources collected and power consumed by the swarm are monitored. When any of the degradation coefficients of a given robot drops below a minimum threshold, d_0 , that robot is declared as faulty and returns itself to the base. By varying

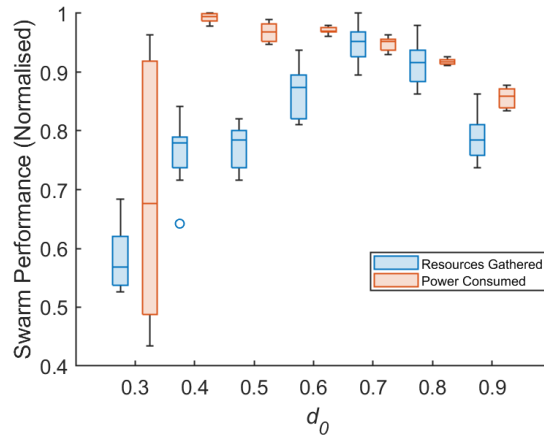


Figure 3. The resources collected and power consumed in 15 minutes by a SRS of $N = 10$ robots performing Algorithm 1. Each robot is given a random probability (1 - 15%) of d_l , d_r and d_s decreasing by 0.01 each second of simulated time. Maintenance is scheduled at varying degradation thresholds, d_0 . Data presented is normalised to a common y axis.

the value d_0 , an appropriate point for maintenance scheduling can be found. The normalised results across 5 experimental replicates are plotted in Figure 3.

Figure 3 shows that setting d_0 in the range $0.7 \leq d_0 \leq 0.8$ produces the best performance in terms of total resources collected per experiment, with $d_0 = 0.7$ offering marginally better performance. Scheduling at $d_0 > 0.8$ results in more frequent interruptions to normal operation, while the physical effects of degradation are more obstructive at $d_0 < 0.7$. In terms of power consumed, unsurprisingly, the system consumes more power the longer it is left to degrade. For $d_0 \leq 0.3$, some robots become stuck, unable to complete the return journey to base. This is why there is a sharp decrease in the total resources collected, and also the power consumed – since robots that are unable to return to base are also unable to continue consuming power once their batteries are fully depleted.

$d_0 = 0.75$ is selected as the target for autonomous detection of degradation and maintenance scheduling. The effects of motor failure in the scenario considered here are far more severe than sensor failure, which exerts a comparatively benign influence on Figure 3. This is because sensing range is non-critical to the foraging behaviour described by Algorithm 1 until $r \leq 0.75$. However, for the purposes of experimentation, a target of $d_0 = 0.75$ for detecting sensor degradation is retained since there are other SRS/MRS scenarios where sensor range could be critical to overall success (e.g. where a swarm must self-localise).

4. Model of Artificial Antibody Population Dynamics

In order to autonomously detect degradation in robot sensor and motor hardware for any value $d_{l,r,s} < d_0$ while remaining tolerant of robots with all values $d_{l,r,s} \geq d_0$, where $d_0 = 0.75$, models of the natural immune system are used as a source of inspiration.

There are two key features of the natural immune system that are desirable to capture in autonomous fault tolerance systems. One is the immune systems ability to remember and more effectively combat familiar infection on subsequent encounter. The other is the immune system's ability to tolerate its host's own cells.

The natural immune system comprises an exceedingly large repertoire of lymphocytes (a type of white blood cell) that recognise and combat infection [24]. When the immune system encounters foreign infection, the lymphocytes that recognise pathogens proliferate and differentiate [24]. Once the infectious cells are destroyed, the immune cells which most effectively fought the infection are retained as memory cells [25]. These cells enable a faster and more efficient immune response should the host encounter the same infection again [26]. If the immune system conflates infectious and domestic cells, it can potentially kill its host –

known as *autoimmunity* [27]. Immune network theory [28] supposes that any lymphocyte can itself be recognised by a sub-section of the total lymphocyte repertoire, and that it is these domestic interactions that occur in the absence of any infectious cell that result in self-tolerance as an emergent property of the immune system.

Model of Antibody Population Dynamics

Discussion of immunological models requires the use of immunological terminology that may be unfamiliar in other fields of research. For ease of reading, a list of frequently used terms is provided alongside definitions which, although highly simplified, aim to provide an intuitive understanding of the models described.

- Antibody: Produced by the host's own immune cells for the purpose of detecting infectious cells.
- Antigen: Produced by infectious cells. To be detected and destroyed by immune cells.
- 'Lock and Key' binding: Antibodies bind to antigens and each other according to the complimentary shapes of the paratopes and epitopes of each.
- Paratope: The part of an antibody or antigen that recognises during binding.
- Epitope: The part of an antibody or antigen that is recognised during binding.
- Matching specificity: The strength of binding between a paratope and epitope.

Farmer, Packard, and Perelson [8] use immune network theory as the basis for their simplified immune model, consisting of a set of differential equations for modelling antibody concentrations, given by Equation 4.1.

$$\dot{x}_i = c \left[\sum_{j=1}^{N_x} m_{ji} x_i x_j - k_1 \sum_{j=1}^{N_x} m_{ij} x_i x_j + \sum_{j=1}^{N_y} m_{ji} x_i y_j \right] - k_2 x_i \quad (4.1)$$

Where there are N_x antibody types, with concentrations $\{x_1, x_2, \dots, x_{N_x}\}$ and N_y antigen types, with concentrations $\{y_1, y_2, \dots, y_{N_y}\}$. The first term represents the stimulation of antibody type x_i when its paratope recognises the epitope of antibody type x_j . The second term represents the suppression of antibody type x_i when its epitope is recognised by the paratope of antibody type x_j . The third term is the stimulation of antibody type x_i when its paratope recognises the epitope of antigen y_j . m_{ij} and m_{ji} are the binding specificities between paratopes and epitopes of type i and j . c and $k_{1,2}$ are tuning parameters. The final term indicates that the antibody populations decay proportionally if they do not interact.

Equation 4.1 reduces the complexity of natural immune processes to the interactions between paratopes and epitopes of antibodies and antigens. Simplified, when an antibody recognises and binds to another antibody or antigen, its concentration increases in proportion to the strength of recognition. When an antibody is recognised and bound by another antibody, its concentration decreases in proportion to the strength of binding. Antibody repertoire diversity and self-tolerant equilibrium is achieved through mutual self-interactions in the first two terms, while the third term prompts additional stimulation of antibodies that bind to antigens. Paratopes and epitopes are represented as variable 1D binary strings of length l_p and l_e , respectively, which can interact in a variety of possible alignments and orientations. $s = \min(l_e, l_p)$ is defined as the matching threshold, below which antibodies do not interact. The strength of binding between epitope i and paratope j , or matching specificity, m , is given by Farmer et al. [8] as Equation 4.2.

$$m_{ij} = \sum_k G \left[\sum_n e_i(n+k) \wedge p_j(n) - s + 1 \right] \quad (4.2)$$

Where $e_i(n)$ denotes the value of the n^{th} bit of the i^{th} epitope string, and $p_j(n)$ the n^{th} bit of the j^{th} paratope string. $G(x) = x$ for $x > 0$, and $G(x) \approx 0$ otherwise. The sum over n ranges over all possible positions on the epitope and paratope; the sum over k allows the epitope to be shifted with respect to the paratope. G measures the strength of a possible reaction between the epitope and the paratope. For a given k , $G = 0$ if less than s bits are complementary, otherwise G is equal to the number of complementary bits in excess of the threshold s plus one (Equation 4.2). If matches occur at more than one alignment, their respective strengths are summed.

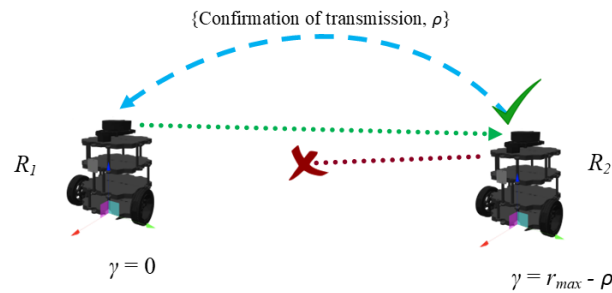


Figure 4. An illustration of determining the value γ . Robot R_1 emits a simulated transmission for localising. The signal is received by R_2 , which then computes the relative location of R_1 and shares this information via a separate simulated communication channel. Since there are no instances of R_1 receiving a transmission from a robot that is unable to confirm R_1 's own transmission, R_1 has $\gamma = 0$. R_2 receives an outgoing signal transmission from R_1 , enabling it to position R_1 at a distance of δ . but does not receive confirmation that R_1 has received the outgoing transmission from R_2 because the transmission range of R_2 has dropped. R_2 therefore sets $\gamma = r_{max} - \rho$.

Constructing Artificial Antibodies

Applying Equation 4.1 and Equation 4.2 to autonomous fault tolerance, robot behavioural signatures are mapped to paratopes of artificial antibodies and antigens. For the fault implementation described in section 3, degraded motor hardware will affect robot linear velocity, v , angular velocity, ω , and power consumption, ΔP . Whereas degraded motor hardware produces readily and endogenously measurable effects in each robot according to the values of $d_{l,r}$ so long as the robot is moving, the effects of degraded sensor hardware are not always easily observable. Previous studies show that the the number of detected objects in range (e.g. walls, other robots, etc.) are among the most effective metrics in detecting sensor failures [29]. Recalling the implementation of sensor degradation described in Section 3, d_S only affects the transmission range – i.e. a degraded robot would be able to detect and localise a perfectly functioning robot up to 4m away, but the perfect robot would not be able to localise the degraded robot. Therefore, in order to monitor the degradation of signal transmission range, a type of handshake protocol is used – when robot R_1 receives a localising transmission from robot R_2 , R_1 sends a message over a separate communication channel (as used in [20]) to confirm its receipt of transmission to R_2 and its estimated Euclidean distance, ρ , from R_2 and vice versa. In the event that R_1 receives confirmation that its transmission was received by R_2 , but R_2 does not receive confirmation from R_1 , R_2 writes the distance estimated from R_1 's transmission to variable γ such that $\gamma = r_{max} - \rho$. This process is illustrated in Figure 4. Where multiple robots provide multiple values of γ , the largest is taken. If all robots are able to successfully complete the handshake, or if no other robots are within their own respective sensing ranges, $\gamma = 0$. γ thus encodes the shortest distance at which the mutual handshake between two robots fails. Artificial antibody populations corresponding to motor hardware, x_M , and sensor hardware, x_S , are handled separately.

There is a large combination and range of possible values of v , ω , ΔP , and γ according to the values $0 \leq d_{l,r,s} \leq 1$. This limits the usefulness of the binary encoding used by Farmer et al. (Equation 4.2) that has since been applied in previous fault tolerant SRS works (e.g. [12], [6]) to indicate true or false statements about robot behaviour – e.g. whether linear velocity is greater than a threshold value. Instead, it is the shapes of v , ω and ΔP , or γ , plotted over time, that are used to represent the paratopes of artificial antibodies and antigens (see Figure 5).

Each robot constantly monitors and records its own sensor readings to a rolling window, W , of the n most recent recordings is used for analysis. Previous work employing this approach in hardware implements W such that it contains approximately 30-50 seconds worth of recorded data [12] [17]. Depending on robot behaviour, much of the information collected may be redundant (e.g. if the robot moves in a straight line for the entire time). The data in W , containing the 300 most recent readings of v , ω , ΔP , and γ , corresponding to 50 seconds of simulated time, is split into smaller parts of length $l = 30$, each representing 5 seconds of

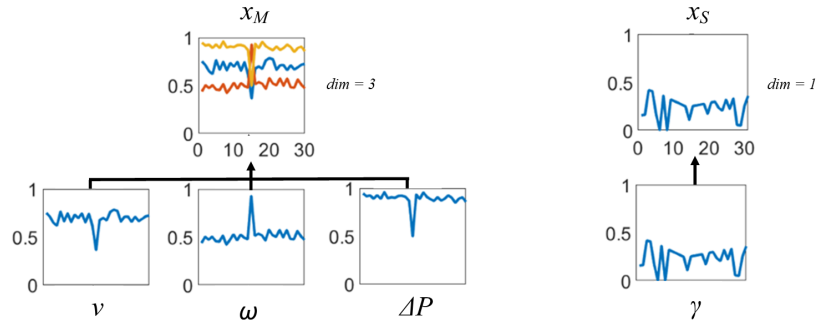


Figure 5. The construction of artificial antibodies for monitoring the performance of robot motors, x_M , and sensors, x_S . x_M has a 3 dimensional paratope consisting of 5 second recordings ($l=30$) of robot linear velocity, v , angular velocity, ω , and rate of power consumption, ΔP . x_S has a 1 dimensional paratope consisting of a 5 second recording of γ .

recorded data. Each part then represents the paratope of an artificial antibody type x_i and is added to the robot's antibody repertoire \mathbf{X} .

Farmer et al. [8] express the matching specificity between a paratope and an epitope as Equation 4.2. Since the paratope of an artificial antibody is represented by a plot over time, rather than a physical object, its perfectly matching epitope would follow the same plot. The distinction between paratopes and epitopes of artificial antibodies are therefore not considered in the AAPD-model presented in this section. However, for descriptive continuity, the binding sites of artificial antibodies and antigens are both referred to as paratopes. The similarity, or matching specificity, m , between two artificial paratopes, p_i and p_j , is given by summing the residuals of the two paratopes convolved over one another and averaging. This is described by Equation 4.3 and illustrated in Figure 7.

$$m(p_i, p_j) = \frac{1}{dim} \sum_{dim} \frac{1}{|\kappa|} \sum_{\epsilon \in \kappa} G[s - \sum_n^{\eta} [p_i(n) - p_j(n)]] \quad (4.3)$$

Where dim is the number of dimensions used to construct the paratope - i.e. $dim = 3$ for a paratope of x_M encoding v , ω , and ΔP , $dim = 1$ for a paratope of x_S encoding γ . Each dimension is normalised in the range $[0,1]$. η is the number of overlaying data points between two artificial paratopes. n is the index of data points in the overlapping range η . k is the maximum number of allowable datapoints that are overhanging or mismatched as two paratopes are convolved over one another. κ is the set of all points of convolution such that $\epsilon \in \kappa = 0 : g : \tau$ where $\tau = \|p_i\| - \|p_j\| + k + 1$. For $k=0$, two paratopes of equal size will only have one possible convolution point from which a residual can be taken - e.g. $\tau = 1$. For mismatched paratope sizes, the number of possible points of convolution is determined by the difference in size and the maximum allowable offset k . The value g can be set at 1 to give a comprehensive convolution across every possible value, or increased to give a sparser convolution at decreased computational cost. Terms G and s are used to enforce a matching threshold. $G(x) = x$ for $x > 0$, and $G(x) = 0$ otherwise. As the sum of residuals between p_i and p_j approaches 0, $G(x)$ approaches s . If the summed residuals are greater than s , matching is considered insufficient to be counted and is discarded. Equation 4.3 is functionally parallel with Equation 4.2 used by Farmer et al. [8].

Implementation of the AAPD Model on SRS

The following describes the distributed implementation of the AAPD model across a SRS. Consider a SRS performing Algorithm 1. Robot states v , ω , and ΔP , or Σ are recorded at a rate of 6Hz. When a robot has collected l readings, they are used to create the paratope of a new artificial antibody. Each time a new artificial antibody is created it is added to the robot's repertoire \mathbf{X} unless an artificial antibody already

exists in the repertoire with a similar paratope. The similarity of artificial antibody paratopes is given by Equation 4.3.

Once all robots have recorded sufficient data points to fill their respective behavioural windows, W , the AAPD model can perform a computation. Recalling the first two terms in Equation 4.1, the first term, representing the stimulation of an antibody type x_i when it recognises antibody x_j , and the second term, representing the suppression of antibody type x_i when it is recognised by the antibody x_j . These are the interactions between self, in the absence of any foreign antigen, that lead to the immune system's self-tolerance as an emergent property. This can be equated to a model of outlier detection that exploits robot multiplicity. For each robot, the paratope of each artificial antibody in repertoire \mathbf{X} is matched to the robot's own behavioural window, W_{self} , according to Equation 4.3, and the population of each artificial antibody stimulated according to the strength of matching. This has the effect of providing greater stimulation to artificial antibody populations with paratopes that are persistently exhibited by the robot and less to those that are only exhibited momentarily. Each robot also compares each of its artificial antibody paratopes to the behavioural windows, $W_{1-(N-1)}$, of every other robot in communication range. If the paratope of an artificial antibody matches strongly with the behavioural windows of other robots, its population is suppressed. This process for a given artificial antibody population x_i can be expressed as: Equation 4.4.

$$\dot{x}_i = c[m(p_i, W_{self}) - k_1 \sum_{j=1}^{N-1} m(p_i, W_j)] - k_2 \quad (4.4)$$

Where x_i is the population level of an artificial antibody with paratope p_i . c and $k_{1,2}$ are tuning coefficients. The final term, k_2 , enforces suppression of the antibody population if it is unreactive. Equation 4.4 functions as an online outlier detection model and represents the 'zeroth order' implementation of the AAPD model. If artificial antibody population x_i drops below zero, it is removed from repertoire \mathbf{X} . If the population of artificial antibody x_i is stimulated above fault threshold f , such that $x_i > f$, it is treated as indicative of a fault in the robot to which it belongs. That robot then returns itself to base for receiving maintenance before being redeployed. Upon returning to base, any artificial antibody populations for which $x > f$ have their paratopes added to a repertoire of artificial antigens, \mathbf{Y} , before being removed from the robot's artificial antibody repertoire \mathbf{X} . A new antigen is only added to \mathbf{Y} if \mathbf{Y} does not already contain an artificial antigen with a strongly matching paratope. Artificial antigens can then be introduced into future calculations of \dot{x}_i . Where a given artificial antibody paratope p_i matches with an artificial antigen paratope p_j , the population of x_i is additionally stimulated according to the specificity of the strongest matching artificial antigen paratope, resulting in quicker detection and mimicking the learning and memorisation properties of the natural immune system. This also allows the AAPD model to perform diagnosis if an artificial antigen paratope is associated with a particular type of fault. Whereas each robot keeps its own private artificial antibody repertoire, the artificial antigen repertoire is shared across the swarm with each new addition so that all robots benefit from the learning process. Artificial antigens are never removed from \mathbf{Y} once added. The AAPD model for first order implementations and higher can now be described by Equation 4.5.

To address the use of AAPD model 'order' terminology used in this section and beyond: An instance of the AAPD model that is not provided with an artificial antigen repertoire is considered a zeroth order model. If an instance of the AAPD model is provided with an artificial antigen repertoire collected during a zeroth order implementation, then the new instance of the AAPD model is considered to be first order. If another instance of the AAPD model is then provided with an artificial antigen repertoire collected during a first order implementation, this is now considered to be second order, and so on (Figure 6).

$$\dot{x}_i = c[m(p_i, W_0) \cdot (1 + k_3 \max(m(p_i, \mathbf{Y}))) - k_1 \sum_{j=1}^N m(p_i, W_j)] - k_2 \quad (4.5)$$

There are some differences in implementation between Equation 4.5 and Equation 4.1. Early experimentation revealed that implementing the antigen stimulation as a separate term to be summed (the third term in Equation 4.1) created scenarios whereby an artificial antibody that was exhibited momentarily but closely matched an artificial antigen could drive a positive feedback loop and result in a large number of false positive detections. Instead, Equation 4.5 attaches the artificial antigen term as a coefficient to the

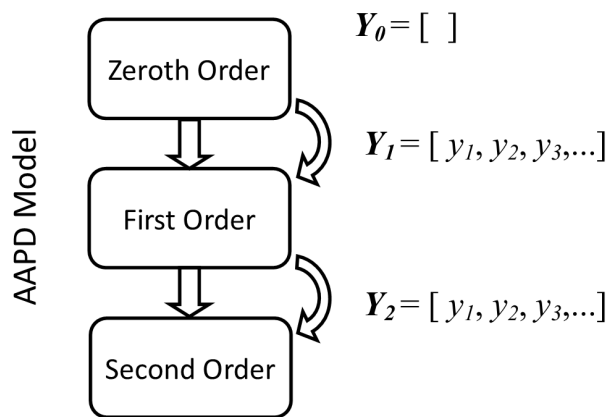


Figure 6. An illustration of the relationship between AAPD model order and its artificial antigen repertoire. The order of an AAPD model that is provided with a non-empty artificial antigen repertoire Y is one greater than the order of the AAPD model used to produce Y

artificial antibody self-stimulation term, meaning that a given paratope must always be present in a robots behavioural window W for any stimulation to occur. Similarly, the decision to take the maximum matching specificity from antigen repertoire Y , rather than summing over all antigens in the repertoire, is informed by the challenge in regulating the degree of stimulation from summing over repertoires that can be highly variable in size and contents.

A simplified illustration of the AAPD model can be seen in [Figure 7](#).

Parameter Selection

Parameters selection aims to produce an AAPD model that stimulates the populations of artificial antibodies produced by robots with any value $d_{l,r,S} < 0.75$ above threshold f , while remaining tolerant of the populations of artificial antibodies produced by robots with all values $d_{l,r,S} > 0.75$. A SRS of $N = 10$ robots performing Algorithm 1 is considered where robot R_1 is initialised with a probability between 5-15% of $d_{l,r,S}$ decrementing by 0.01 per second of simulated time while robots R_{2-10} are initialised with $0.75 < d_{l,r,S} < 1$ (similar to the experiment described in section 3). Optimising model parameters for this situation was surprisingly challenging - early efforts to use gradient descent were unsatisfactory, mostly because of the difficulty in defining an appropriate quantitative fitness measure. The performance of the AAPD model can be broadly assessed by the maximisation of true positive and the minimisation of false positive detections. The objective of the AAPD model is to detect when any of R_1 's decrementing $d_{l,r,S}$ values drop below 0.75, and so this can be set as the true positive condition with all other instances of detection considered false positive. In practice, there is not enough behavioural distinction between, for example, a robot with $d_l = 0.74$ and a robot with $d_l = 0.76$ to achieve this reliably - especially if d_r remains high. Setting any instance of fault detection where $d_{l,r,S} > 0.75$ as a false positive instance and punishing those parameter combinations during the gradient descent process results in model parameters that struggle to detect true positive instances until $d_{l,r,S}$ are much lower than desired. This illustrates that the boundary between true and false positive detection is much more difficult to define for a sliding scale of degradation - especially where multiple degradation coefficients contribute to overall behaviour as with d_l and d_r . For example, detecting a fault for a robot where $d_{l,r,S} = 0.76$ is preferable to detecting at $d_{l,r,S} = 0.6$ if the ideal point of detection is $d_0 = 0.75$. The persistence of detection must also be factored in. In general, the closer the value of $d_{l,r,S}$ at the moment of detection, δ , is to d_0 , and the longer the AAPD model can sustain a true positive detection thereafter, the better. However, there is a distinction between model behaviours that should be actively punished vs. those that should merely be improved upon. For example, detecting a fault once a robot is at $d_{l,r,S} = 0.3$ and sustaining the detection thereafter is not ideal. However, this is nonetheless

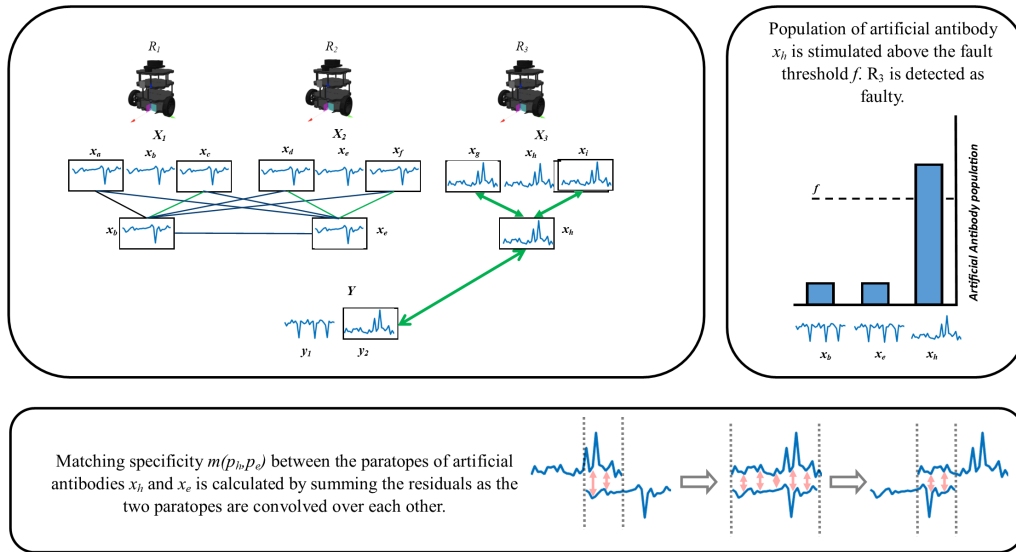


Figure 7. The AAPD-model runs on a TurtleBot3 SRS (robots R_{1-3} shown). Small temporal samples of robot state and sensor data (linear velocity shown) are encoded in artificial antibodies, for which each robot has its own repertoire (\mathbf{X}_{1-3}). R_1 's artificial antibody x_b has a high matching specificity, m , with antibodies x_d and x_e according to Equation 4.3, resulting in stimulation of population x_b . The same is true for R_2 's antibody x_e with x_d and x_f . The high matching specificity between the artificial antibodies of R_1 and R_2 (x_b with x_d , x_e , and x_f , and x_e with x_d , x_b , and x_c) results in the mutual suppression of populations of x_b and x_e such that they are tolerated as normal. R_3 's artificial antibody x_h has a high matching specificity with artificial antibodies x_g and x_i , resulting in population stimulation of x_h , however x_h has a low matching specificity with the antibodies of R_1 and R_2 because of the high residuals when they are convolved with Equation 4.3, meaning that the population of x_h is not suppressed. x_h is further stimulated by its high matching specificity with artificial antigen y_2 which further stimulates the population of x_h , taking it over the threshold f for detection of R_3 as faulty.

a true positive detection that the AAPD model should be able to make reliably and should not therefore be punished too severely by the learning process. Detecting a fault at $0.76 < d_{l,r,S} < 0.8$ is a false positive detection that is arguably undeserving of punishment by the learning process, since it falls within the ideal range shown in Figure 3. If the model makes a false positive detection for, e.g., $d_{l,r,S} = 0.95$, but only momentarily, the punishment should also be less severe than if the detection was sustained. It is very difficult to meaningfully quantify and offset the contributions of true positives, false positives, and the persistence of each without understanding the costs (e.g. time, energy expense, resources gained/lost, etc.) of robot operation, robot repair, and objective values which, while highly relevant to the field of autonomous fault tolerance research, require knowledge of a specific robot platform and use-case scenario which are beyond the scope of this study. Parameter values were instead user-selected via a qualitative approach, aiming to maximise true positive detection, minimise false positive detections, but remain tolerant of false positives for values of $d_{l,r,S}$ close to 0.75. The parameters tuned were s in Equation 4.3, and k_{1-2} in Equation 4.5. $k_{1,2}$ were tuned with a granularity of 0.01, while s was tuned with a granularity of 0.1. This process revealed that different stages of the AAPD model performed better with different values of s in Equation 4.3. In all cases, the size of behavioural windows $|W| = 300$, the size of artificial antibody paratopes $l = 30$, and the fault threshold $f = 1$. For determining whether new artificial paratopes are added to repertoires \mathbf{X} or \mathbf{Z} with Equation 4.3, $s = 1.5$ and $k = 20$.

Experimentation revealed that parameter values of the AAPD model that performed well for artificial antibody repertoire \mathbf{X}_M did not necessarily perform comparably for repertoire \mathbf{X}_S and vice versa. The

Process	Computation	s	g	k	k_1	k_2	k_3
Adding to \mathbf{X} or \mathbf{Y}	Equation 4.3	1.5	1	10	-	-	-
$\mathbf{X}_M:W$ matching	Equation 4.3	4	5	0	-	-	-
$\mathbf{X}_M:\mathbf{Y}_M$ matching	Equation 4.3	1.5	1	10	-	-	-
\mathbf{X}_M population dynamics	Equation 4.5	-	-	-	0.24	0.3	1.2
$\mathbf{X}_S:W$ matching	Equation 4.3	5	5	0	-	-	-
$\mathbf{X}_S:\mathbf{Y}_S$ matching	Equation 4.3	3.3	1	10	-	-	-
\mathbf{X}_S population dynamics	Equation 4.5	-	-	-	0.18	0.3	1.2

Table 2. The various parameter selections for Equation 4.5 and Equation 4.3 used within different stages of the AAPD model

decision was therefore made to handle repertoires \mathbf{X}_M and \mathbf{X}_S with separate instances of the AAPD model, each with their own parameter selections.

The matching specificity between the paratope of an artificial antibody in repertoire \mathbf{X}_M and robot behavioural windows W is determined with Equation 4.3 where $s = 4$, $g = 5$, and $k = 0$. The matching specificity between the paratope of an artificial antibody in repertoire \mathbf{X}_M and the paratope of an artificial antigen in repertoire \mathbf{Y}_M is determined with Equation 4.3 where $s = 1.5$, $g = 1$, and $k = 10$. The population of artificial antibodies in repertoire \mathbf{X}_M is governed by Equation 4.5 where $k_1 = 0.24$, $k_2 = 0.3$, and $k_3 = 1.2$.

The matching specificity between the paratope of an artificial antibody in repertoire \mathbf{X}_S and robot behavioural windows W is determined with Equation 4.3 where $s = 5$, $g = 5$, and $k = 0$. The matching specificity between the paratope of an artificial antibody in repertoire \mathbf{X}_S and the paratope of an artificial antigen in repertoire \mathbf{Y}_S is determined with Equation 4.3 where $s = 3.3$, $g = 1$, and $k = 10$. The population of artificial antibodies in repertoire \mathbf{X}_S is governed by Equation 4.5 where $k_1 = 0.18$, $k_2 = 0.3$, and $k_3 = 1.2$.

For ease of reference, this information is summarised in Table 2.

5. Experiments, Results & Discussion

10 replicates were performed for each experimental scenario described in this section. Note that experiments concerned with motor faults and sensor faults are conducted separately (i.e. $d_S = 1$ when $d_{l,r}$ are variable and vice versa) and complete separation is maintained between model orders (i.e. an artificial antigen paratope added to repertoire $\mathbf{Y}_{M,S}$ will not be provided to the AAPD model during the same experiment or in any other experiment with an AAPD model of the same order. Total robot power is set to $P_{max} = \infty$ for all experiments in this section except those described in the final subsection. The reason for this is so that robots do not completely deplete their power during experiments where this would be unhelpful for assessing model performance.

The performance of the AAPD model is assessed on the following principal criteria:

- δ : The smallest value of $d_{l,r}$ or the value of d_S at the moment an artificial antibody population is first stimulated above threshold f and a robot is detected as faulty.
- Ψ_T : True positive detection rate, or the experimental time during which a robot is detected at faulty as a proportion of the total time it spends with one or more degradation severity coefficients $d_{l,r,S} \leq 0.75$
- Ψ_F : False positive detection rate, or the experimental time during which a robot is detected at faulty as a proportion of the total time it spends with all degradation severity coefficients $d_{l,r,S} > 0.75$

Degradation in a Single Robot

The first scenario used to test the AAPD model is identical to that described for the parameter selection process in the previous section. Namely, from a SRS of $N = 10$ robots, robot R_1 is initialised with $0.9 < d_{l,r,S} < 1$ with independent probabilities between 5-15% of $d_{l,r,S}$ decrementing by 0.01 per second while

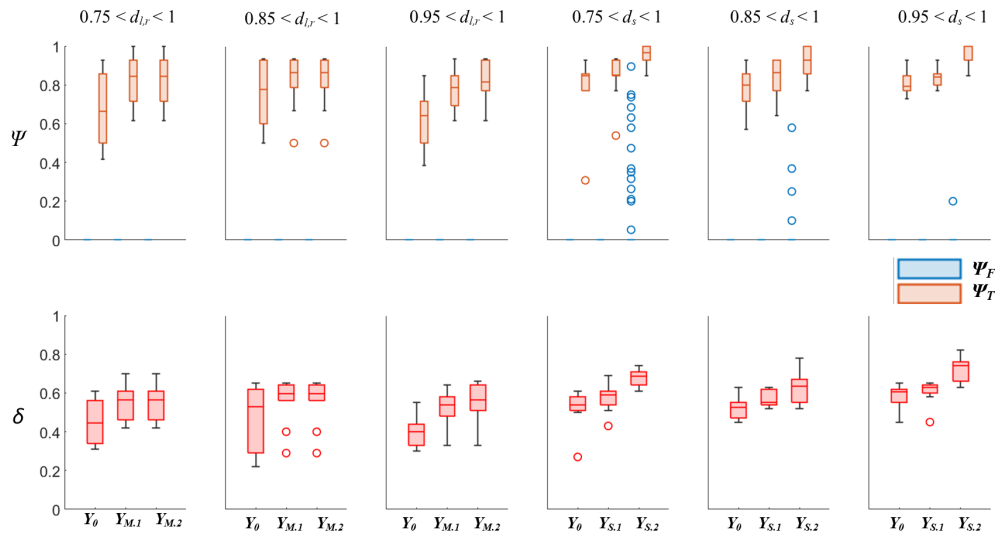


Figure 8. Ψ_T (red), Ψ_F (blue), and δ for zeroth, first, and second order AAPD models, denoted Y_0 , $Y_{M,1,S,1}$, or $Y_{M,2,S,2}$, respectively, on SRS of $N = 10$ robots. In the leftmost three columns, AAPD models operate on \mathbf{X}_M . Robot R_1 is initialised with $0.9 < d_{l,r} \leq 1$ and a random probability between 5-15% of $d_{l,r}$ decrementing by 0.01 per second of simulated time. Robots R_{2-10} are initialised with $d_{l,r}$ in various sub-ranges of $[0.75, 0.85, 0.95] < d_{l,r} \leq 1$. In the rightmost three columns, AAPD models operate on \mathbf{X}_S . Robot R_1 is initialised with $0.9 < d_s \leq 1$ and a random probability between 5-15% of d_s decrementing by 0.01 per second of simulated time. Robots R_{2-10} are initialised with d_s in various sub-ranges of $[0.75, 0.85, 0.95] < d_s \leq 1$.

robots R_{2-10} are initialised with static $0.75 < d_{l,r,S} < 1$. The performance of the zeroth, first, and second order AAPD Model is assessed.

The zeroth and first order AAPD models operating on \mathbf{X}_M and \mathbf{X}_S in this scenario are used to produce the following artificial antigen repertoires. Note that the experiments used to produce artificial antigen repertoires are separate from the experiments conducted to assess AAPD model performance.

- $Y_{M,1}$ contains artificial antigen paratopes produced by robots detected as faulty by the zeroth order AAPD model operating on \mathbf{X}_M over 10 experimental replicates, and contains a total of 99 unique paratopes.
- $Y_{M,2}$ contains artificial antigen paratopes produced by robots detected as faulty by the first order AAPD model provided with $Y_{M,1}$ operating on \mathbf{X}_M 101 unique paratopes.
- $Y_{S,1}$ contains artificial antigen paratopes produced by robots detected as faulty by the zeroth order AAPD model operating on \mathbf{X}_S over 10 experimental replicates, and contains a total of 93 unique paratopes.
- $Y_{S,2}$ contains artificial antigen paratopes produced by robots detected as faulty by the first order AAPD model provided with $Y_{S,1}$ operating on \mathbf{X}_S over 10 experimental replicates, and contains a total of 109 unique paratopes.

Figure 8 displays the Ψ_T , Ψ_F and δ for the zeroth (denoted Y_0), first, and second order AAPD models, provided with artificial antigen repertoires $Y_{M,1,S,1}$ and $Y_{M,2,S,2}$, respectively, operating on \mathbf{X}_M and \mathbf{X}_S for swarms of $N = 10$ robots. Robot R_1 is initialised with $0.9 < d_{l,r,S} \leq 1$ and a random probability between 5-15% of $d_{l,r,S}$ decrementing by 0.01 per second of simulated time. Robots R_{2-10} are initialised with static $0.75 < d_{l,r,S} < 1$, $0.85 < d_{l,r,S} < 1$, and $0.95 < d_{l,r,S} < 1$. This is done in order to assess how the coverage of $d_{l,r,S}$ values among R_{2-10} affects AAPD model performance.

	\mathbf{X}_M									\mathbf{X}_S								
	$0.75 < d_{l,r} < 1$			$0.85 < d_{l,r} < 1$			$0.95 < d_{l,r} < 1$			$0.75 < d_s < 1$			$0.85 < d_s < 1$			$0.95 < d_s < 1$		
	\mathbf{Y}_0	$\mathbf{Y}_{M,1}$	$\mathbf{Y}_{M,2}$	\mathbf{Y}_0	$\mathbf{Y}_{M,1}$	$\mathbf{Y}_{M,2}$	\mathbf{Y}_0	$\mathbf{Y}_{M,1}$	$\mathbf{Y}_{M,2}$	\mathbf{Y}_0	$\mathbf{Y}_{S,1}$	$\mathbf{Y}_{S,2}$	\mathbf{Y}_0	$\mathbf{Y}_{S,1}$	$\mathbf{Y}_{S,2}$	\mathbf{Y}_0	$\mathbf{Y}_{S,1}$	$\mathbf{Y}_{S,2}$
ψ_T	0.67	0.85	0.85	0.78	0.86	0.86	0.64	0.79	0.82	0.85	0.85	0.97	0.80	0.86	0.93	0.79	0.84	1
ψ_F	0	0	0	0	0	0	0	0	0	0	0	0	0	0	0	0	0	0
δ	0.45	0.57	0.57	0.53	0.60	0.60	0.4	0.54	0.57	0.54	0.59	0.69	0.53	0.55	0.64	0.61	0.63	0.74

Table 3. The median values of each boxplot displayed in Figure 8

Figure 8 shows that, for both \mathbf{X}_M and \mathbf{X}_S , there is little consistency in the impact of the coverage of $d_{l,r,S}$ among R_{2-10} on ψ_T , ψ_F , or δ . The only exception to this is a slight improvement in the performance of the AAPD operating on \mathbf{X}_S where R_{2-10} are initialised with $0.95 < d_s \leq 1$. One explanation for this is in the implementation of degradation in this work, shown in Figure 2, where the sigmoidal function and inverse square relationship mean that the change in output is lowest in the range $0.75 < d_{l,r} < 1$ (except for the rate of power consumption, ΔP). This also provides explanation as to why the swarm foraging performance declines once $d_0 < 0.7$ in Figure 3. Interestingly, this is the range where the ΔP is the most responsive to changes in $d_{l,r}$. There is thus an opportunity for ΔP to provide a more effective means of early fault detection, but the present insensitivity of the AAPD model to ΔP alone suggests that it may need greater weighting in the matching specificity calculations (Equation 4.3) to achieve the desired effect.

The first order AAPD model operating on \mathbf{X}_M gives a notable improvement from the zeroth order model in all cases, while the additional improvement offered by the second order AAPD model is much-reduced. Contrastingly, the first order AAPD model operating on \mathbf{X}_S offers some improvement over the zeroth order model, but there is a far more pronounced improvement by the second order AAPD model at the expense of higher ψ_F . This behaviour is explained principally by the difference in paratope dimension of artificial antibodies in repertoire \mathbf{X}_M and \mathbf{X}_S and the difference in values of s when matching artificial antibody and antigen paratopes. \mathbf{X}_M consists of artificial antibodies with 3 dimensional paratopes comprised of v , ω , and ΔP . While these metrics are each related to one another, there are many combinations of values they can assume depending on the values of $d_{l,r}$ and an element of randomness in the sign of ω (normalised to < 0.5 or > 0.5) according to the direction of turn. This means there is overall more variation in the paratopes contained in \mathbf{X}_M , resulting in reduced self-stimulation of any given paratope in any given window W , on average. The additional stimulation provided by $\mathbf{Y}_{M,1}$, even with a relatively low $s = 1.5$ that limits additional stimulation only to those paratopes with very close matches, means that the artificial antibody populations that may have been insufficiently exhibited for the zeroth order AAPD model to stimulate are now picked up much more quickly by the first order model. However, because of the scope for variation within \mathbf{X}_M , the strict matching specificity requirements imposed by $s = 1.5$, and the fact that the AAPD computation only updates every 50 seconds of simulated time (i.e. each time W has refreshed), it is largely the same artificial antibody populations that are stimulated above threshold f at the same computation cycle by the second order AAPD model, and so there is little added benefit. On the other hand, \mathbf{X}_S is made up of artificial antibodies with 1 dimensional paratopes containing only γ . Although γ can vary quickly as robots pass in and out of sensing range of one another, it does not provide \mathbf{X}_S with the stability of paratopes consisting of multiple semi-independent dimensions. Furthermore, increased values of s were needed to produce satisfactory performance from the AAPD model when matching the paratopes of artificial antibody populations with W and with antigen repertoire \mathbf{Y}_S , with $s = 5$ and $s = 3.3$, respectively. This means that paratopes contained in \mathbf{X}_S are less constrained by the requirement for a close match, resulting in antibody populations in \mathbf{X}_S being additionally stimulated and detected by the AAPD model at higher values of d_s across all model orders when compared to \mathbf{X}_M . Figure 8 reveals a potential problem for single dimension paratopes and the AAPD model. The first order AAPD model, when operating on \mathbf{X}_S , produces a relatively muted improvement in performance. This is perhaps because, as with the second order AAPD operating on \mathbf{X}_M , the majority of artificial antibody populations that are stimulated above threshold f by the first order AAPD model are the same and occur at the same computation cycle as in the zeroth order AAPD model. However, there is some improvement, meaning that some new paratopes, corresponding to higher values of d_s , are added to repertoire \mathbf{Y}_S . Each paratope in \mathbf{Y}_S will produce matching specificity with

any paratope in \mathbf{X}_S according to the value of s . One can imagine this in d_S space, such that a paratope where $d_S = n$ will approximately match with any other paratope for which d_S falls in some range $n \pm q(s)$ where $q(s)$ represents some function of s . Since paratopes in \mathbf{Y}_S are 1 dimensional, each time a new paratope with a higher d_S is added, the matching space $n \pm q(s)$ also increases without the counterbalances provided by additional dimensions. This is what results in the second order AAPD model operating on \mathbf{X}_S picking up a relatively large amount of false positive artificial antibody populations, particularly where R_{2-10} are initialised with $0.75 < d_S \leq 1$. One possible mitigating solution to this problem would be including additional paratope dimensions – received signal strength could be a useful candidate in this scenario. Alternatively offsetting the additional stimulation produced by artificial antigen paratopes corresponding to learned models of faults with additional suppression corresponding to learned models of normal behaviour.

Figure 8 and Table 3 demonstrate the learning ability of the AAPD model, with first and second order models improving the Ψ_T from as low as 64% to as much as 86% in \mathbf{X}_M , or from 79% to 100% in \mathbf{X}_S . This learning is unsupervised and entirely based on a data-driven model of outlier detection. Referring to Figure 3, cases of robots being unable to return themselves to base after detection were not observed until $d_{l,r} \leq 0.3$. The fact that, in this scenario, the zeroth order AAPD model operating on \mathbf{X}_M is able to keep δ in the range $0.4 \leq \delta < 0.53$ is a promising result. It is interesting that, even for first and second order models, the median average δ for true positive detections by the AAPD model could not be brought above 0.6 without introducing large amounts of false positive detections. This, again, may be an issue with the sigmoidal fault modelling and equal weighting of paratope dimensions – the matching of linear velocity, v , and angular velocity, ω , which are relatively unresponsive in the range $0.75 < d_{l,r} < 1$, contribute twice as much as the matching of the more responsive power consumption term, ΔP . Nonetheless, Figure 3 shows that a minimum $d_{l,r} = 0.6$ at the moment of detection is sufficient for the swarm to retain autonomy with only a 10% reduction in median performance from the optimum. Additionally, the AAPD model operating on \mathbf{X}_S performs better across all orders and scenarios and is shown in Table 3 to achieve ideal median performance for the second order AAPD model where R_{2-10} are initialised with $0.95 < d_S \leq 1$.

Multiple Degrading Robots & Varying Swarm Size

The next set of experiments differ slightly insofar that when a robot is detected as faulty it is reset and reinitialised with its original $d_{l,r,S}$ values. This process is instantaneous (i.e. the faulty robot does not need to return itself to the safe zone, although experiments with this physical constraint are described later in this section) in order to focus on the AAPD models response to swarms of varying size and composition. Since the number of other robots directly affects the suppression term in Equation 4.5, k_2 is defined proportionally to the number of robots, N , such that $\hat{k}_2 = k_2(\frac{10}{N})$ where \hat{k}_2 assumes the value of k_2 in Equation 4.5 during a given experiment.

Figure 9A plots the values of δ for robots detected as faulty by zeroth, first, and second order AAPD models operating on \mathbf{X}_M for SRS where $2 \leq N \leq 10$. First and second order AAPD models are provided with $\mathbf{Y}_{M,1}$ and $\mathbf{Y}_{M,2}$, respectively. True positive detections are shown in red, while false positives are shown in blue. Robot R_1 is initialised with $0.9 < d_{l,r} < 1$ and a probability between 5 - 15% of $d_{l,r}$ decrementing by 0.01 per second of simulated time, while robots R_{2-N} are initialised with static $0.75 < d_{l,r} \leq 1$. The frequency of true positive and false positive detections across all experimental replicates are also plotted in the rightmost column of Figure 9A. Figure 9B shows the same information and scenarios as Figure 9A but for the AAPD model operating on \mathbf{X}_S as d_S decrements in R_1 over time with first and second order AAPD models provided with $\mathbf{Y}_{S,1}$ and $\mathbf{Y}_{S,2}$, respectively. Figure 9C plots the values of δ for robots detected as faulty by zeroth, first, and second order AAPD models operating on \mathbf{X}_M for SRS where $N = 10$ but multiple robots can degrade at the same time. Between 1 - 10 robots are initialised with $0.9 < d_{l,r} < 1$ and a probability between 5 - 15% of $d_{l,r}$ decrementing by 0.01 per second of simulated time, while the remaining robots out of the 10 are initialised with static $0.75 < d_{l,r} \leq 1$. Figure 9D shows the same information and scenarios as Figure 9C but for the AAPD model operating on \mathbf{X}_S as d_S decrements in some proportion of robots over time.

Figure 9A-B show that the AAPD is insensitive to changes in the swarm size above a certain point. The zeroth order AAPD model achieves a relatively consistent rate of true positive detections with false positive instances mostly eliminated once for swarm sizes $N \geq 4$, beyond which adding more robots produces no

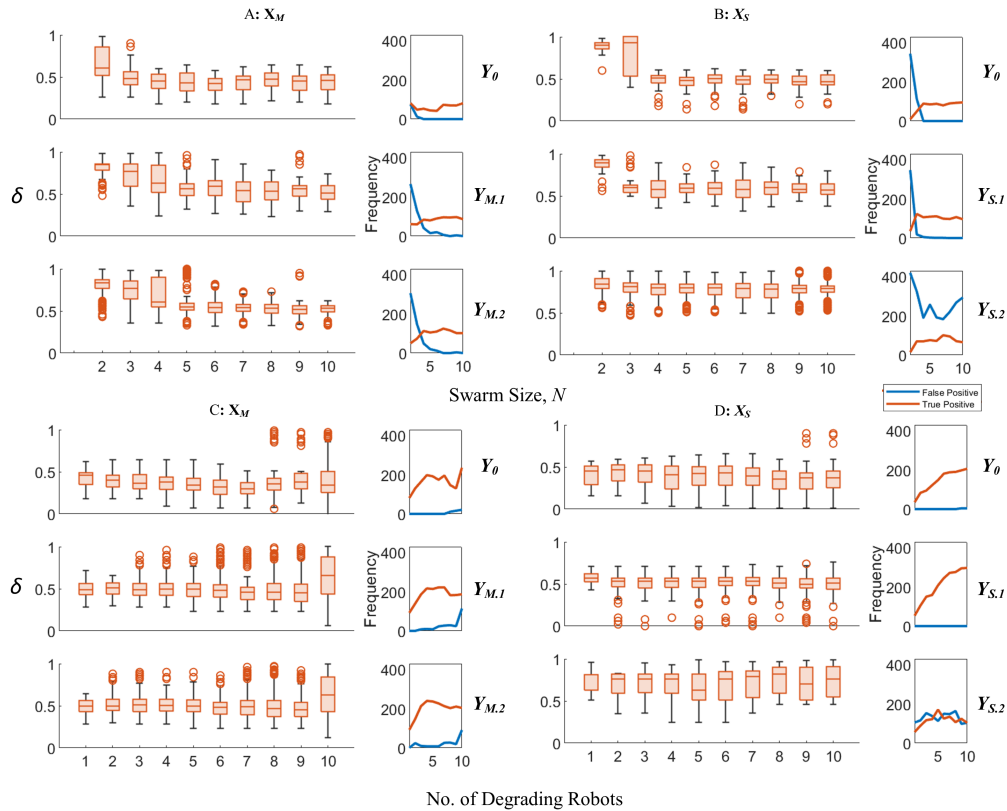


Figure 9. δ for robots detected as faulty by zeroth (denoted Y_0), first, and second order AAPD models, provided with artificial antigen repertoires $Y_{M,1,S,1}$ and $Y_{M,2,S,2}$, respectively. The summed frequency of true positive (red) and false positive (blue) detections across all experimental replicates are also plotted alongside each scenario. **A:** AAPD models operate on X_M for different SRS sizes N . R_1 is initialised with $0.9 < d_{l,r} < 1$ and a probability between 5 - 15% of $d_{l,r}$ decrementing by 0.01 per second of simulated time, while robots R_{2-N} are initialised with static $0.75 < d_{l,r} \leq 1$. **B:** AAPD models operate on X_S for different SRS sizes N . R_1 is initialised with $0.9 < d_S < 1$ and a probability between 5 - 15% of d_S decrementing by 0.01 per second of simulated time, while robots R_{2-N} are initialised with static $0.75 < d_S \leq 1$. **C:** AAPD models operate on X_M for SRS where $N = 10$. Between 1 - 10 robots are initialised with $0.9 < d_{l,r} < 1$ and a probability between 5 - 15% of $d_{l,r}$ decrementing by 0.01 per second of simulated time, while the remaining robots are initialised with static $0.75 < d_{l,r} \leq 1$. **D:** AAPD models operate on X_S for SRS where $N = 10$. Between 1 - 10 robots are initialised with $0.9 < d_S < 1$ and a probability between 5 - 15% of d_S decrementing by 0.01 per second of simulated time, while the remaining robots are initialised with static $0.75 < d_S \leq 1$.

consistent change to overall performance for both X_M and X_S . This result demonstrates the scalable potential of the AAPD model insofar that a larger SRS would not necessarily require each robot to perform larger computations simply because there were more robots if comparable results can be achieved with a smaller sub-population. Performance plateau occurs for $N \geq 5$ robots for first and second order AAPD models operating on X_M – although false positives are not completely eliminated for $N > 5$, the frequency of the false positives is very small above this point (i.e. less than one per experiment on average). The first order AAPD model operating on X_S also achieves stability for swarm sizes $N \geq 4$, but converges more quickly than the zeroth order model. However, the second order AAPD model operating on X_S never reaches a stable point and maintains a high rate of false positive detections for all swarm sizes. Looking at the frequency of true positive and false positive detections, which are approximately equal in each entry,

one can infer that there is an approximately equal probability of any detection made by second order AAPD model operating on \mathbf{X}_S of being true or false. This is because of the effect previously described, whereby a 1 dimensional artificial antigen paratopes increases the corresponding values d_S of the artificial antibody paratopes it will match with on each successive model order. However, this effect appears to be much more severe in Figure 9B than in Figure 8. The reason for this is that Figure 8 shows false positive as a proportion of total experimental time, whereas Figure 9B shows the frequency of false positive detections in a robot. This reveals that, although the second order AAPD model operating on \mathbf{X}_S may detect as many false positives as true positives, it is more likely to retain true positive detections over successive computations.

Figure 9C-D again shows that the AAPD model exhibits a high degree of stability for its zeroth order implementation. As expected, increasing the proportion of degrading robots in the swarm produces an increase in the frequency of true positive detections (although this comes with a reduction in the median δ and an increased interquartile range) for both \mathbf{X}_M and \mathbf{X}_S . The frequency of false positive detections for the zeroth order AAPD model remains consistently low. The first and second order AAPD models increase the values of δ in all scenarios. For the first order AAPD model operating on \mathbf{X}_S , this benefit comes at no expense. When operating on \mathbf{X}_M the benefits of the first order AAPD model are eventually offset by increased instances of false positive detection. For swarms with up to 5 simultaneously degrading robots, the frequency of false positive detections are minimal for \mathbf{X}_M – a positive result that exemplifies the promise of the AAPD model’s self tolerance, learning, and memory functions. The frequency of false positive detections increases once the majority of the swarm (6+) are simultaneously degrading, accompanied by a small decrease in true positive detections resulting from the fact that fewer robots are given the opportunity to reach $d_{l,r} < 0.75$. This is to be expected, given that it can already be seen from Figure 9A that a minimum number of robots with $0.75 < d_{l,r} \leq 1$ is needed to maintain robust classification. This number is 5 robots for the first and second order AAPD models, and so it follows logically that the performance of these models would deteriorate once the guarantee of 5 or more robots in the non-faulty range is removed, as is seen in Figure 9C, since the system no longer retains a robust majority-model of normal operation. This produces a compound negative effect on the AAPD model performance, firstly; the potential for several robots with $d_{l,r} < 0.75$ to simultaneously exhibit similar artificial antibody paratopes increases the population suppression of these paratopes and delays their detection as faulty until they occupy a sufficiently unique behavioural space. Secondly; the possibility for a majority of robots to operate with $d_{l,r} < 0.75$ and a minority with $d_{l,r} > 0.75$ means that non-faulty robots can be correctly identified as outliers, but erroneously detected as faulty. The primary cause of false positive detection in Figure 9C is the loss of a robot majority population with $d_{l,r} > 0.75$ combined with additional stimulation provided by \mathbf{Y}_M and the fact that artificial antibody paratopes do not substantially change in the range $0.75 < d_{l,r} < 1$. This combined means that an artificial antigen paratope taken from a robot with, for example, $d_{l,r} \approx 0.75$, can provide the extra stimulation needed to take a non-faulty artificial antibody population over the fault threshold f if its population is not adequately suppressed by the remainder of the swarm. The unsuitability of the second order AAPD model operating on \mathbf{X}_S in this scenario is again observed, while the second order AAPD model operating on \mathbf{X}_M offers small improvements in median δ and frequency of false positive detections where greater proportions of the SRS degrade simultaneously.

Overall Figure 9 shows that the AAPD model is able to reliably maintain the performance shown in Figure 8 and Table 3 for SRS comprising as few as 4 robots and where up to half the total population are degrading simultaneously. In general, the unsupervised selection of artificial antigen paratopes works well – an encouraging result for the AAPD model as part of a closed-loop unsupervised autonomous system. However, potential problems with the unsupervised selection process and low paratope dimensions are also highlighted that are first in need of address.

Diagnosis

The distinctive shapes of artificial antibody paratopes are suited to fault diagnosis as well as detection. This study considers SRS with two classes of failure – motor failure and sensor failure. These two classes are orthogonal in fault space for the implementation described here (i.e. a fault in a robot’s motor does not directly affect the reliability of the robot’s sensor and vice-versa). Therefore, when a true positive fault detection is made by the AAPD model, the robot to which the artificial antibody population $x_i > f$ belongs is

identified as faulty, and can be identified as having a motor or sensor fault according to whether x_i belongs to \mathbf{X}_M or \mathbf{X}_S . Provided that the detection is a true positive, this information will always be correct and provides an innate diagnostic function to the AAPD model across all orders.

More challenging is the diagnosis of faults within classes that are interactive and variable. An example of this would be diagnosing which motor has failed out of many. In the SRS studied here, this amounts to determining whether the left, right, or both motors are degraded. This is more challenging than diagnosing orthogonal faults, since each motor exerts influence on shared artificial antibody paratope dimensions. For example, $\omega \approx 0$ for motors at any stage of degradation so long as their stages of degradation are approximately equal. Similarly, two moderately healthy motors can have the same collective ΔP as a robot with one motor in perfect condition and the other severely degraded. The shape of the paratope across all dimensions is therefore critical to the sub-class diagnosis of faults.

The proposed mechanism for sub-class diagnosis is only available to the AAPD models at the first order and above. Recalling that, when an artificial antibody population is stimulated above the fault threshold f and the robot it belongs to is detected as faulty, it returns itself to the base to receive any necessary maintenance. This study assumes that, as part of the maintenance process, the true nature of any degradation can be revealed, either in supervised fashion by a trained human operator or unsupervised via the types of diagnostic test proposed in [6]. Thus, paratopes added to artificial antigen repertoires can be associated with an appropriate sub-class repair action(s) – e.g., in this case, replacement of left, right, or both motors – that provides a ground truth to the nature of the fault. Now, when a first order AAPD model operates on \mathbf{X}_M , it does so with an artificial antigen repertoire \mathbf{Y}_M containing paratopes that are labelled with sub-class diagnostic information. When an artificial antibody population is then stimulated above threshold f , the artificial antigen paratope it matched most strongly with can also be used to perform sub-class diagnose of the fault.

To test this capability, a SRS of $N = 10$ robots, R_{1-10} , perform Algorithm 1. R_1 is initialised with $0.9 < d_{l,r} < 1$ with independent probabilities between 5-15% of $d_{l,r}$ decrementing by 0.01 per second, while R_{2-10} are initialised with static $0.75 < d_{l,r} < 1$. A first order AAPD model provided with $\mathbf{Y}_{M,1}$ operates on \mathbf{X}_M . Each paratope in $\mathbf{Y}_{M,1}$ is labelled with one of the following categories:

- Category 1: Both motors require maintenance ($d_l \leq 0.75$ and $d_r > 0.75$).
- Category 2: Left motor requires maintenance ($d_l \leq 0.75$ and $d_r > 0.75$).
- Category 3: Right motor requires maintenance ($d_l > 0.75$ and $d_r \leq 0.75$).
- Category 4: False positive ($d_l > 0.75$ and $d_r > 0.75$).

Figure 10A displays a pie chart representing the true makeup of detection categories made by a first order AAPD model provided with provided with $\mathbf{Y}_{M,1}$ as a proportion of the total number of detections over 10 experimental replicates. Figure 10B shows the rates of correct/incorrect diagnoses made by the AAPD model as a proportion of the total number diagnostic attempts over the same 10 experimental replicates.

Figure 10A shows that 75% of all detections made by the first order AAPD model operating on \mathbf{X}_M occur when both $d_l \leq 0.75$ and $d_r \leq 0.75$. This is to be expected given that both d_l and d_r degrade simultaneously and Figure 9 shows that the average δ at the moment of detection in this scenario is 0.55, by which point it is common that both $d_{l,r} \leq 0.75$. Nonetheless, a substantial minority is accounted for by single motor failure, with only a very small number of false positives.

Figure 10B shows that, in 79% of all cases, the artificial antigen paratope that most strongly matches with the paratope of an artificial antibody population stimulated above the fault threshold yields a correct sub-class diagnosis, with only 12% being incorrect. In fact, 79% is an underestimate, since 9% of all diagnoses were false-positive detections. Removing these instances from consideration, the proportion of correct diagnoses becomes 87%, with 13% incorrect. The reason that false-positive detections account for 9% of diagnoses but only 2% of total detections is that many instances of true positive detection by the AAPD operating on \mathbf{X}_M , shown in Figure 10A, occur in the absence of a strongly matching artificial antigen paratope, cannot therefore be diagnosed to a sub-class level, and so cannot be shown in Figure 10B.

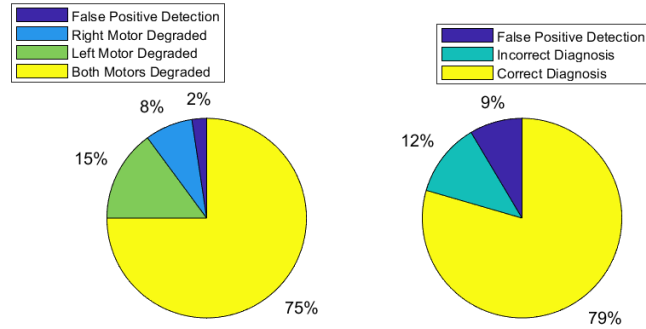


Figure 10. A: The categories of faults detected by the first order AAPD model (provided with $\mathbf{Y}_{M,1}$) operating on \mathbf{X}_M as a proportion of all faults detected over 10 experimental replicates. **B:** The correct and incorrect sub-class diagnoses by the first order AAPD model using $\mathbf{Y}_{M,1}$ as a proportion of all diagnostic attempts over 10 experimental replicates.

Spontaneous Faults and Environmental Variations

Assessment of the AAPD model has so far focused on gradual degradation in robots. While this is an important and understudied mode of failure in fault tolerant literature in MRS/SRS, there are nonetheless scenarios in which failure can occur spontaneously, or sudden onset environmental changes can produce similar effects.

The first set of experiments in this section considers the types of spontaneous electro-mechanical failure studied in previous swarm fault tolerance literature (e.g. [30]). The implementation of these faults is as follows:

- Complete failure of both motors, $H_1: d_l = 0$ and $d_r = 0$
- Complete failure of a single motor, $H_2: d_l = 0$ while $0.75 < d_r \leq 1$
- Complete failure of sensor, $H_3: d_S = 0$

In the following experiments, SRS of sizes $2 \leq N \leq 10$ performing Algorithm 1 for 15 minutes of simulated time are studied. Robot R_1 is initialised with one of the fault types H_{1-3} , while robots R_{2-N} are initialised with $0.75 < d_{l,r,S} < 1$. The robot data collected is used to test the performance of the AAPD model offline.

The zeroth order AAPD model operating on \mathbf{X}_M and \mathbf{X}_S in this scenario is used to produce two new artificial antigen repertoires, $\mathbf{Y}_{M,C}$ and $\mathbf{Y}_{S,C}$, respectively. $\mathbf{Y}_{M,C}$ contains artificial antigen paratopes produced by robots detected by the zeroth order AAPD model as suffering H_1 or H_2 over 10 experimental replicates, and contains a total of 11 unique paratopes. $\mathbf{Y}_{S,C}$ contains artificial antigen paratopes produced by robots detected by the zeroth order AAPD model as suffering H_3 over 10 experimental replicates, and contains a total of 14 unique paratopes. The vast reduction in the number of paratopes in $\mathbf{Y}_{M,C,S,C}$ compared with $\mathbf{Y}_{M,1,M,2,S,1,S,2}$ is indicative of the relative simplicity of complete failures H_{1-3} – such failures should be easy to detect among a normally functioning SRS. Second order AAPD models were found to perform identically to first order models when detecting H_{1-3} , and so they are omitted from further discussion.

Figure 11 plot Ψ_T and Ψ_F for the zeroth and first order AAPD models operating on \mathbf{X}_M and \mathbf{X}_S with varying N . First order AAPD models operating on \mathbf{X}_M and \mathbf{X}_S are provided with $\mathbf{Y}_{M,C}$ and $\mathbf{Y}_{S,C}$.

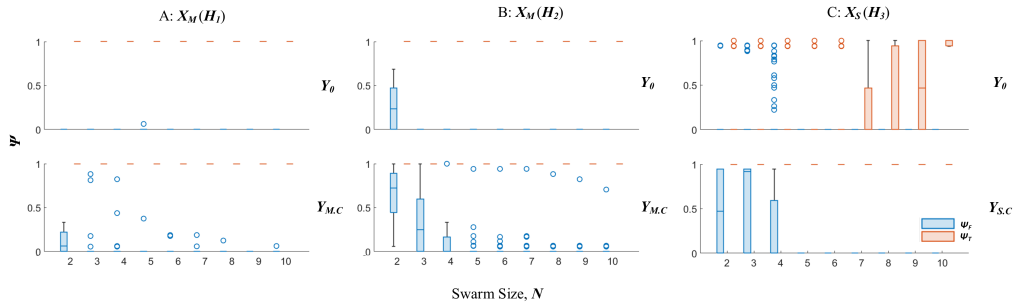


Figure 11. AAPD model performance, Ψ_T (red) and Ψ_F (blue), for varying SRS sizes, N , where robot R_1 is initialised with complete failure type (H_{1-3}) and R_{2-N} are initialised with $0.75 < d_{l,r,S} \leq 1$. **A:** Zeroth order AAPD model operating on \mathbf{X}_M where R_1 suffers H_1 . **B:** First order AAPD model provided with $\mathbf{Y}_{M,C}$ operating on \mathbf{X}_M where R_1 suffers H_1 . **C:** Zeroth order AAPD model operating on \mathbf{X}_M where R_1 suffers H_2 . **D:** First order AAPD model provided with $\mathbf{Y}_{M,C}$ operating on \mathbf{X}_M where R_1 suffers H_2 . **E:** Zeroth order AAPD model operating on \mathbf{X}_S where R_1 suffers H_3 . **F:** First order AAPD model provided with $\mathbf{Y}_{S,C}$ operating on \mathbf{X}_S where R_1 suffers H_3 .

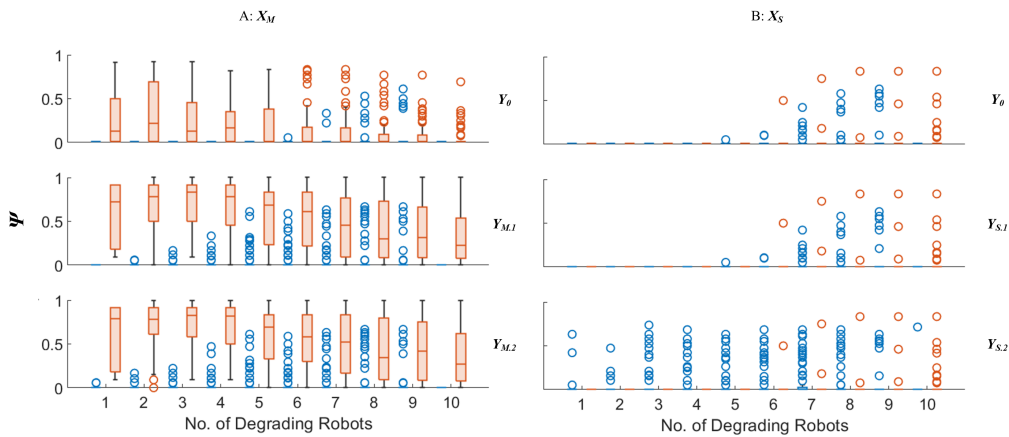


Figure 12. A: Ψ_T (red) and Ψ_F (blue) for zeroth, first, and second order ($\mathbf{Y}_{M,1}$ and $\mathbf{Y}_{M,2}$) AAPD models operating on \mathbf{X}_M . **B:** Ψ_T and Ψ_F for zeroth, first, and second order ($\mathbf{Y}_{S,1}$ and $\mathbf{Y}_{S,2}$) AAPD models operating on \mathbf{X}_S .

respectively. Figure 11A-D shows that the AAPD model operating on \mathbf{X}_M is able to correctly detect robots with H_1 or H_2 while remaining tolerant of non-faulty robots for the entire experiment duration where the swarm consists of 5 or more robots for zeroth and first model orders. For all values of N , the zeroth and first order AAPD model operating on \mathbf{X}_M correctly detects H_1 and H_2 at all times, leaving no room for improvement of Ψ_T by the first order model, which serves only to increase the median false positive detection rate for smaller swarm sizes. Figure 11E-F show that the zeroth order AAPD model operating on \mathbf{X}_S struggles to detect H_3 in R_1 with consistency until $N = 10$. The first order model provided with $\mathbf{Y}_{S,C}$ thus gives a clear improvement to the detection of H_3 . The reason for the relatively poor performance by the zeroth AAPD order operating on \mathbf{X}_S . at lower N is that R_1 spends proportionally more time outside the sensing range of the other robots it needs to obtain a reading for $\gamma > 0$ and so the nature of the fault is obscured from the AAPD model.

The next set of experiments focuses on sudden but tolerable changes in robots and their environment and how they are handled by the AAPD model. With comprehensive prior knowledge and characterisation of robot behaviours, it is often possible to detect deviations from normal operation with a simple thresholding model. For example, if $\Delta P \approx \Delta P_{max}$ while moving in a straight line, this could be used to detect degradation in motors $d_{l,r}$, possibly closer to the ideal $d_{l,r} \approx 0.75$ than the median $d_{l,r} \approx 0.6$ achieved by the AAPD model. The drawback with such an approach, however, is inflexibility. If an environmental variation, such as a change in surface friction or lateral wind, were to result in a comparable increase in the rate of power consumption, this could result in high levels of false-positive fault detections. Ideally, a fault detection system should be tolerant of environmental fluctuations within a safe range (i.e. where the robot's autonomy is not threatened), but detect whether continued operation is likely to result in near-term failure. The complexity of this challenge is compounded by the interaction space between environmental variations and the degradation of robot hardware

The following experiment considers a SRS of $N = 10$ robots, R_{1-10} , initialised with static $0.75 < d_{l,r} < 1$ performing 1 for 15 minutes of simulated time. After 5 minutes of simulated time, between 1 and 10 robots in the swarm have their respective $d_{l,r,S}$ values instantly degraded to $\frac{2}{3}$ of their initial value, where they remain until the end of the experiment (all other robots remain with their respective $d_{l,r}$ values unchanged). The robot data collected is used to test the performance of the AAPD model offline. Figure 12A plots Ψ_T and Ψ_F for the zeroth and first order AAPD models operating on \mathbf{X}_M . The first and second order AAPD models are provided with $\mathbf{Y}_{M,1}$ and $\mathbf{Y}_{M,2}$. Figure 12B shows the equivalent information for AAPD models operating on \mathbf{X}_S , where first and second order AAPD models are provided with $\mathbf{Y}_{S,1}$ and $\mathbf{Y}_{S,2}$.

Figure 12A shows that the AAPD model operating on \mathbf{X}_M maintains a very low Ψ_F rate, with median zero across all scenarios. It can be seen that there are some outlying instances where robots are falsely detected as faulty for relatively large proportions of experimental time, and that these are most frequent for cases where the majority (but not all) of the swarm degrades since these are the scenarios in which the mutual suppression of remaining robots with $0.75 < d_{l,r} < 1$ will be least. For the zeroth order AAPD model, Ψ_T decreases as the proportion of degraded robots increase up to and above a majority population. Where degraded robots are in the minority, the zeroth order AAPD gives a wide range of Ψ_T values that appear to be substantially reduced from those presented in Table 3. However, it must be remembered that Table 3 presents data taken from a gradually degrading robot which, once detected, will typically only become easier to detect as it degrades further. Figure 12, on the other hand, shows data from robots that remain at $\frac{2}{3}$ of their initialised $d_{l,r}$ values which, in many cases, will be higher than the δ values in Table 3, meaning that many of the degraded robots are tolerated by the AAPD model or have their artificial antibody populations stimulated above f only momentarily.

The first and second order AAPD models operating on \mathbf{X}_M provided with $\mathbf{Y}_{M,1}$ and $\mathbf{Y}_{M,2}$, respectively, give a higher median Ψ_T across all scenarios and, in most cases, with a smaller inter-quartile range. For cases where a majority of robots degrade, however, the inter-quartile range of Ψ_T remains relatively large with a low median, indicating that the majority of degraded robots are tolerated as a result of mutual suppression among the SRS.

Figure 12B shows that the AAPD model operating on \mathbf{X}_S is overwhelmingly tolerant to sensor degradation of robots in the range $0.5 < d_S < 0.66$, with median $\Psi_T = 0$ and $\Psi_F = 0$ for all cases. Larger populations of degraded robots results in more outlying non-zero instances of Ψ_T and Ψ_F by the zeroth order model. This is most likely down to chance, where there will be a relatively small number of paratopes that a robot can exhibit that are not tolerated by the AAPD model, and the probability of these paratopes being present during any given AAPD model computation increases with increasing populations of robots with $0.5 < d_S < 0.66$. It also increases the opportunity for a relatively small number of paratopes exhibited by robots with $0.75 < d_S \leq 1$ to be detected as faulty since there are fewer robots with corresponding artificial antibody paratopes to suppress them. Such is the AAPD model's tolerance to robots with $0.5 < d_S < 0.66$ that $\mathbf{Y}_{S,1}$ has no observable effect on $\Psi_T = 0$ or $\Psi_F = 0$. The unreliability of $\mathbf{Y}_{S,2}$ has already been demonstrated in Figure 9, and so the increased number of outlying $\Psi_{T,F}$ values are not taken to be indicative of an improved model performance.

Overall, the ability of the AAPD model to detect or tolerate the degraded robots shown in Figure 12 is neither inherently positive or negative, and model parameters were not selected with this scenario in mind. Nonetheless, what is demonstrated in Figure 12 is that the AAPD model, according to its parameter values,

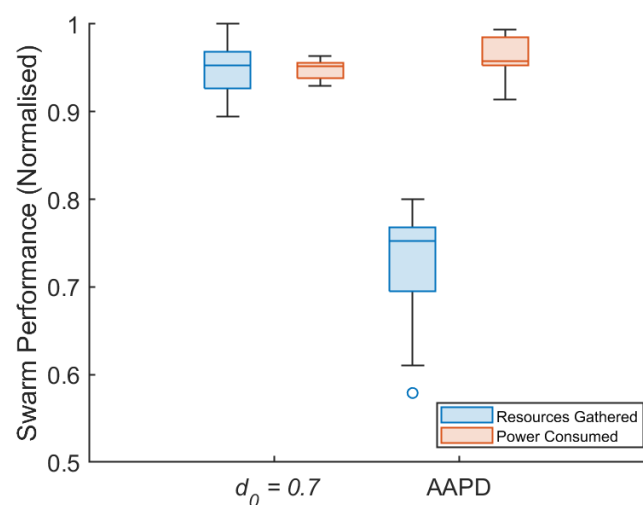


Figure 13. The resources collected and power consumed in 15 minutes by a SRS of $N = 10$ robots performing Algorithm 1. Each robot is given a random probability (1 - 15%) of d_l , d_r and d_s decreasing by 0.01 each second of simulated time. Performance is shown for an SRS that can automatically detect faults with $\delta = d_0$ where $d_0 = 0.7$ alongside an SRS running a second order AAPD model provided with $Y_{M,2}$ operating on X_M and a first order model provided with $Y_{S,1}$ operating on X_S . Data presented is normalised to a common y axis.

can detect reductions in performance affecting minority populations of robots while remaining tolerant of the same reductions affecting majority populations at the zeroth order. In a real world scenario this would potentially allow the AAPD model to tolerate substantial shifts in behaviour brought about by environmental changes that affect the majority of robots. The detection of such shifts affecting a minority of robots could also be exploited in mapping and path planning. For example, if a minority of robots are persistently detected as faulty when moving into a particular area, that area could be bounded as a no-go zone or given an additional cost weighting when planning optimal routes between destinations. There is ultimately a limit to the usefulness of tolerating system wide effects caused by environmental variations. If continued operation in a particular environment threatens robot autonomy, it should be identified and mitigated – even if the entire system is affected. At higher orders, the AAPD model is able to detect reductions in performance even where they affect majority populations if they result in artificial antibody populations with paratopes that match sufficiently with an artificial antigen paratope. A well calibrated AAPD model, then, could potentially recognise unsustainable operating conditions and overcome corresponding mutual suppression even when a majority of robots are affected.

Foraging Performance

For the final assessment of the AAPD model, the experiment from Section 3 is repeated. A SRS of $N = 10$ robots perform Algorithm 1 for 15 minutes of simulated time. Robots R_{1-10} are each initialised with independent and random probabilities between 1 - 15% of $d_{l,r,s}$ decrementing by 0.01 per second of simulated time. Each robot’s power is returned to $P_{max} = 1$ during these experiments. The best performing AAPD models for motor and sensor faults are deployed across the SRS. For the AAPD model operating on X_M , a second order model provided with $Y_{M,2}$ is used. For the AAPD model operating on X_S , a first order model provided with $Y_{S,1}$ is used. Figure 13 plots the overall SRS performance, in terms of the number of resources collected and the power consumed, when the models are deployed, alongside the performance for $d_0 = 0.7$ from Figure 3 for comparison.

Figure 13 shows that implementation of the highest performing AAPD models result in a median swarm performance that is approximately equivalent to perfect fault detection with $\delta = 0.5$. This is an agreement with the results shown in Figure 9, in which the median average $\delta \approx 0.5$ for the second order AAPD model provided with $\mathbf{Y}_{M,2}$ operating on \mathbf{X}_M . The normalised median value for the resources gathered by the swarm is 0.75, with the optimum median for $\delta = 0.7$ at 0.95. The normalised median value for the power consumed by the swarm is 0.95, with the optimum median for $\delta = 0.7$ at 0.96. The implementation of AAPD models thus allows the SRS to operate at a median 79% of its theoretical optimum rate of resource gathering and only marginally above its optimum rate of power consumption. Importantly, across all experimental replicates, there was not a single instance in which a robot was so degraded that it was unable to make the return journey to base by the time it was detected as faulty. It should be remembered that, although there is room to improve the results shown in Figure 13, all robots of a SRS simultaneously degrading at the accelerated rates chosen for this study is a harsh and exaggerated use-case scenario designed to test the limits of the AAPD model. That the AAPD model is nevertheless able to prevent robot failure in the field in the cases tested is an important achievement that is novel among existing fault tolerant SRS literature.

6. Conclusion

This paper presents the bio-inspired AAPD model, a novel model for autonomously detecting and diagnosing faults. The model is inspired by Farmer et al.'s model of antibody population dynamics in the natural immune system [8]. The AAPD model is naturally distributed, demonstrates promising scalable properties, and is implemented and demonstrated in a mostly unsupervised manner on a SRS.

The AAPD model can be implemented as a zeroth order model, a purely online data driven model that exploits SRS multiplicity to construct an implicit model of normal behaviour, but can also be provided with repertoires of artificial antigens corresponding to known fault signatures, typically resulting in improved performance and enabling sub-class fault diagnosis, mimicking the learning and memory functions of the natural immune system.

The AAPD is tested on its ability to detect gradual or sudden degradation of motor or sensor hardware. In cases of gradual motor degradation, the zeroth order AAPD model can detect faults with up to median $\delta = 0.53$ and $\Psi_T = 0.78$. The first order AAPD model improves this to as much as $\delta = 0.6$ and $\Psi_T = 0.86$. In cases of gradual sensor degradation, the zeroth order AAPD model can detect faults with up to median $\delta = 0.61$ and $\Psi_T = 0.85$, improving to as much as $\delta = 0.74$ and $\Psi_T = 1$ for the second order model. With the exception of the second order model operating on \mathbf{X}_S , the AAPD model maintains a very low rate of false positive detections for all other model orders and scenarios. The AAPD model is able to maintain a comparable performance when implemented on SRS with as few as 5 robots, and where up to 50% of the swarm is simultaneously degrading. When the AAPD is deployed on a degrading swarm performing a foraging task, it is able to ensure that overall swarm performance is within 76% of the optimum and with no instances of uncontrolled robot failure in the field.

The AAPD model, as implemented in this work, is able to isolate any detected fault to its corresponding robot within the SRS. If there are multiple artificial antigen repertoires corresponding to different pieces or categories of robot hardware, any detected fault can be isolated to within these categories. Provided that the detected fault is a true positive, diagnosis of the robot and artificial antibody repertoire that the fault belongs to will always be correct. Additionally, the first order AAPD model is demonstrated to be capable of associating the paratopes of artificial antigens with finer stages of diagnosis. Where the first order AAPD model detects a motor fault, it is able to correctly diagnose whether the fault is in the left, right, or both motors in 87% of the cases tested.

The AAPD model demonstrates a strong ability to detect sudden complete failure in motors or sensor hardware, achieving consistent median average $\Psi_T = 1$ and $\Psi_F = 0$ for SRS with as few as 5 robots in all cases tested. The AAPD model also demonstrates the ability to detect or tolerate smaller sudden reductions to motor or sensor performance to varying degrees, depending on model order, the number of robots affected, and whether motors or sensor are affected.

Overall, the AAPD model presented here demonstrates a robust ability to detect a variety of potential faults and hazards – slow hardware degradation, sudden performance changes, and complete failure of hardware components – while remaining tolerant to robots operating in a defined normal range. The

combination of online data-driven and model-based fault detection, as well as the option for supervised and unsupervised selection and labelling of artificial antigens, means that there are many possible ways of configuring and implementing the model according to the needs of a given scenario. The AAPD model covers substantial new ground in the field of swarm fault tolerance. In addition to being a novel bio-inspired fault detection and diagnosis model, it is the first model in SRS to consider gradual degradation of hardware, the first to incorporate immune-inspired real time learning and memory functions in its detection process, and the first to integrate fault detection and fault diagnosis. Although implemented on SRS in this work, the AAPD model has potential application on many other autonomous systems where there is multiplicity – traditional MRS, single robots with many actuators (e.g. quad, hex, octopod robots), and non-robotic systems such as wind farms). In conclusion, the AAPD model makes a valuable contribution to the field of swarm fault tolerance and autonomous fault tolerance in general.

Future Work

Although the AAPD model performs well in many of the scenarios tested, it also leaves room for improvement in others, and vast opportunity for further research and exploration. Future work will examine:

- Alternative data for use in constructing artificial antibody paratopes, and alternative ways of obtaining a matching specificity between them (e.g. trajectory matching algorithms).
- The use of learned paratopes of normal behaviour to counterbalance the increase in false positive detections caused by artificial antigen repertoires in some scenarios.
- Diagnostic differentiation between internal hazards (e.g. hardware degradation), external hazards (e.g. adverse terrain), and byzantine behaviour (e.g. malicious agents).
- Implementation of the AAPD in different robotic systems (e.g. Non-SRS, legged robots, etc.), and robot hardware.
- The introduction of a severity estimation for artificial antibody populations such that robots at greatest risk of failure in the field can be prioritised.
- Comparison with alternative learned approaches for fault detection and diagnosis (e.g. artificial neural networks).

Acknowledgment

This was supported by the Royal Academy of Engineering UK IC Postdoctoral Fellowship award under Grant ICRF2223-6-121.

References

1. Şahin E. 2005 Swarm robotics: From sources of inspiration to domains of application. In *Swarm Robotics* pp. 10–20. Springer Springer Berlin Heidelberg.
2. Winfield AFT, Nembrini J. 2006 Safety in numbers: fault-tolerance in robot swarms. *International Journal of Modelling, Identification and Control* **1**, 30–37.
3. Bjercknes JD, Winfield AFT. 2013 On fault tolerance and scalability of swarm robotic systems. In *Distributed Autonomous Robotic Systems*, pp. 431–444. Springer.
4. Cohen IR. 2000 *Tending Adam's Garden: evolving the cognitive immune self*. Academic Press.
5. Millard AG. 2016 *Exogenous Fault Detection in Swarm Robotic Systems*. PhD thesis University of York.
6. O'Keeffe J, Tarapore D, Millard AG, Timmis J. 2018 Adaptive Online Fault Diagnosis in Autonomous Robot Swarms. *Frontiers in Robotics and AI* **5**, 131.
7. Carlson J, Murphy R. 2003 Reliability analysis of mobile robots. In *2003 IEEE International Conference on Robotics and Automation (Cat. No.03CH37422)* vol. 1 pp. 274–281 vol.1. ([10.1109/ROBOT.2003.1241608](https://doi.org/10.1109/ROBOT.2003.1241608))
8. Farmer JD, Packard NH, Perelson AS. 1986 The immune system, adaptation, and machine learning. *Physica D: Nonlinear Phenomena* **22**, 187–204.
9. Khalastchi E, Kalech M. 2019 Fault detection and diagnosis in multi-robot systems: A survey. *Sensors* **19**, 4019.

10. Khadidos A, Crowder RM, Chappell PH. 2015 Exogenous Fault Detection and Recovery for Swarm Robotics. *IFAC-PapersOnLine* **48**, 2405–2410.
11. Strobel V, Pacheco A, Dorigo M. 2023 Robot swarms neutralize harmful Byzantine robots using a blockchain-based token economy. *Science Robotics* **8**, eabm4636.
12. Tarapore D, Timmis J, Christensen AL. 2019 Fault detection in a swarm of physical robots based on behavioral outlier detection. *IEEE Transactions on Robotics* **35**, 1516–1522.
13. Carneiro J, Leon K, Caramalho Í, Van Den Dool C, Gardner R, Oliveira V, Bergman ML, Sepúlveda N, Paixão T, Faro J, Others. 2007 When three is not a crowd: a crossregulation model of the dynamics and repertoire selection of regulatory CD4+ T cells. *Immunological reviews* **216**, 48–68.
14. Daigle MJ, Koutsoukos XD, Biswas G. 2007 Distributed diagnosis in formations of mobile robots. *IEEE Transactions on Robotics* **23**, 353–369.
15. Carrasco RA, Núñez F, Cipriano A. 2011 Fault detection and isolation in cooperative mobile robots using multilayer architecture and dynamic observers. *Robotica* **29**, 555–562.
16. Kutzer MD, Armand M, Scheid DH, Lin E, Chirikjian GS. 2008 Toward cooperative team-diagnosis in multi-robot systems. *The International Journal of Robotics Research* **27**, 1069–1090.
17. O’Keeffe J, Millard AG. 2023 Hardware Validation of Adaptive Fault Diagnosis in Swarm Robots. In *Conference Towards Autonomous Robotic Systems* p. in press. Springer.
18. Robotis. 2023 Turtlebot3 Overview. <https://manual.robotis.com/docs/en/platform/turtlebot3/overview/>. [Online; accessed 13-September-2023].
19. Bayindir L. 2016 A review of swarm robotics tasks. *Neurocomputing* **172**, 292–321.
20. Maxim PM, Hettiarachchi S, Spears WM, Spears DF, Hamann J, Kunkel T, Speiser C. 2008 Trilateration localization for multi-robot teams. In *Multi-Agent Robotic Systems* vol. 2 pp. 301–307. SCITEPRESS.
21. Qiu Z, Lu Y, Qiu Z. 2022 Review of ultrasonic ranging methods and their current challenges. *Micromachines* **13**, 520.
22. Ranges L Determining Electric Motor Load and Efficiency. .
23. Zhang Y, Zhang C, Wang S, Chen R, Tomovic MM. 2022 Performance Degradation Based on Importance Change and Application in Dissimilar Redundancy Actuation System. *Mathematics* **10**, 843.
24. Owen JA, Punt J, Stranford SA et al.. 2013 *Kuby immunology*. WH Freeman New York.
25. Kindt TJ, Goldsby RA, Osborne BA, Kuby J. 2007 *Kuby immunology*. Macmillan.
26. Floreano D, Mattiussi C. 2008 *Bio-inspired artificial intelligence: theories, methods, and technologies*. MIT press.
27. Langman RE, Cohn M. 2000 Third Round-Editorial Summary. In *Seminars in Immunology* vol. 12 p. 343. [Philadelphia, PA]: WB Saunders,[c1989-.
28. Jerne NK. 1974 Towards a network theory of the immune system.. In *Annales d’immunologie* vol. 125 pp. 373–389.
29. Lee S, Milner E, Hauert S. 2022 A Data-Driven Method for Metric Extraction to Detect Faults in Robot Swarms. *IEEE Robotics and Automation Letters* **7**, 10746–10753.
30. Tarapore D, Christensen AL, Timmis J. 2017 Generic, scalable and decentralized fault detection for robot swarms. *PLoS ONE* **12(8)**: e0182058. <https://doi.org/10.1371/journal.pone.0182058>.